Heliyon 10 (2024) e26746

Contents lists available at ScienceDirect

Heliyon

journal homepage: www.cell.com/heliyon

Research article

Atmospheric aerosol chemistry and source apportionment of PM10 using stable carbon isotopes and PMF modelling during fireworks over Hyderabad, southern India

Pradeep Attri [a], Devleena Mani [a,*], M. Satyanarayanan [b], D.V. Reddy [b], Devender Kumar [b], Siddhartha Sarkar [c], Sanjeev Kumar [c], Prashant Hegde [d]

[a] Centre for Earth, Ocean and Atmospheric Sciences, University of Hyderabad, Telangana 500046, India
[b] CSIR-National Geophysical Research Institute, Hyderabad, Telangana 500007, India
[c] Physical Research Laboratory, Ahmedabad, Gujarat 380009, India
[d] Space Physics Laboratory, Vikram Sarabhai Space Centre, Thiruvananthapuram, Kerala 695021, India

ARTICLE INFO

Keywords:
Aerosol chemistry
Fireworks
Stable carbon isotope
Elemental carbon
Source apportionment

ABSTRACT

This study examined the influence of fireworks on atmospheric aerosols over the Southern Indian city of Hyderabad during festival of Diwali using mass closure, stable carbon isotopes and the EPA-PMF model. Identification of chemical species in day and night time aerosol samples for 2019 and 2020 Diwali weeks showed increased concentrations of NH_4^+, NO_3^-, SO_4^{2-}, K^+, organic carbon (OC), Ba, Pb and Li, which were considered as tracers for fireworks. PM_{10} source apportionment was done using inorganic (trace elements, major ions) and carbonaceous (organic and elemental carbon; OC & EC) constituents, along with stable isotopic compositions of TC and EC. $K^+/Na^+ \sim 1$ and $K^+_{nss}/OC > 0.5$ indicated contribution from fireworks. High NO_3^-, NH_4^+, Na^+, Cl^- and SO_4^{2-} suggested the presence of deliquescent salts NaCl, NH_4NO_3 and $(NH_4)_2SO_4$. TAE/TCE >1 suggested H^+ exclusion, indicating possible presence of H_2SO_4 and NH_4HSO_4 in the aerosols. Ba, Pb, Sb, Sr and Fe increased by 305 (87), 12 (11), 12 (3), 3 (2) and 3 (4) times on Diwali nights, compared to pre-Diwali of 2019 (2020), and are considered as metallic tracers of fireworks. $\delta^{13}C_{TC}$ and $\delta^{13}C_{EC}$ in aerosols closely resembled that of diesel and C_3 plant burning emissions, with meagre contribution from firecrackers during Diwali period. The $\delta^{13}C_{EC}$ was relatively depleted than $\delta^{13}C_{TC}$ and $\delta^{13}C_{OC}$. For both years, $\delta^{13}C_{OC\text{-}EC}$ ($\delta^{13}C_{OC}$ - $\delta^{13}C_{EC}$) were positive, suggesting photochemical aging of aerosols during long-range transport, while for pre-Diwali 2019 and post-Diwali 2020, $\delta^{13}C_{OC\text{-}EC}$ were negative with high OC/EC ratio, implying secondary organic aerosols formation. High toluene during Diwali week contributed to fresh SOA formation, which reacted with precursor ^{12}C, leading to ^{13}C depletions. Eight-factored EPA-PMF source apportionment indicated highest contribution from residue/waste burning, followed by marine/dust soil and fireworks, while least was contributed from solid fuel/coal combustion.

1. Introduction

Short-term anthropogenically induced extreme events like accidental forest fires, waste and crop residue burnings (CRB), traffic

* Corresponding author.
E-mail address: dtiwarisp@uohyd.ac.in (D. Mani).

https://doi.org/10.1016/j.heliyon.2024.e26746
Received 9 November 2023; Received in revised form 11 February 2024; Accepted 19 February 2024
Available online 5 March 2024

congestions and firework events affect the air quality, which impact the human health [1,2]. These episodic events introduce pollutants into the atmosphere, thus altering the physico-chemical characteristics of the ambient aerosols [1–5]. Short-term firework activities are used for the celebration of festivities worldwide. The firecrackers used are composed, mainly, of nitrates of potassium, barium and strontium, chlorate and perchlorate of potassium, along with dust powder, charcoal and other elements like sulphur, aluminium and iron [6–8]. As firecrackers undergo combustion, metal oxides are released into the atmosphere [8–12], together with elemental carbon (EC) [13], black carbon (BC) [4,14], organic carbon (OC) [15] and water-soluble inorganic ions (WSIIs) [9,16–19]. Firecracker burning also influences the formation of secondary organic aerosols (SOAs), due to the condensation of polycyclic aromatic hydrocarbons (PAHs) [20], acetonitrile and oxygenated volatile organic compounds (OVOCs) [21] from the pyrotechnic products in the atmosphere. Condensation nuclei concentrations (CNC) play critical role in the formation of cloud droplets [22] and have been reported to be significantly high during the firework events [20]. The oxidative potential of aerosols during firework burning is higher than that resulting from the traffic sources [23]. Extreme emissions of the particles in such events affect meteorological conditions. Burning of fireworks lead to increase in ambient temperature, as O_3 and NO_2 are formed during combustion [24]. It also affects the radiative forcing in the local atmosphere [25–27].

Post-monsoon period in India, when festival of Diwali occurs with the firework celebrations, coincides with the crop harvesting season and witnesses a rise in the CRB events [28]. A combined effect of CRB and fireworks over Delhi was reported during Diwali [29], primarily due to the air-mass migrating from Punjab and Haryana, along with transboundary movements [19,30]. In the ambient environment, amalgamated effects of different emission sources complicate the evaluation of any specific source, such as fireworks or others, that contribute to the overall emissions. To address this, different techniques have been adopted to apportion individual sources by identification of their physicochemical properties and their contribution and include receptor models like chemical mass balance (CBM), environmental protection agency – positive matrix factorization (EPA-PMF) and principal component analysis (PCA). Various source apportionment techniques are compiled in supplementary data (Table S1). The receptor models require chemical species as inputs to identify different sources. A compilation of studies indicating tracer species for respective sources is presented in supplementary data (Table S2).

Further, the stable carbon isotope compositions of particulate matter (PM) also provide significant insights into the emission sources and transformation processes. In general, the stable isotopic composition of aerosols contributed from combustion of coal (−24.9 to −21 ‰) [31–35], liquid fossil fuel (−28.6 to −24.2 ‰) [36], C_3 (−32 to −20 ‰) and C_4 plants (−17 to −9 ‰) transform considerably, as the aerosols evolve with time in the atmosphere [37]. The influence of atmospheric processes such as photochemical aging and secondary OC (SOC) formation affect the isotopic composition of organic carbon via kinetic isotope effects (KIE) [38].

While majority of aerosol studies in India are reported from the northern (Indo-Gangetic Plain; IGP) and western regions, there are very few comprehensive work [34,39–41] involving chemistry and source apportionments of aerosols over Southern India and further less are the ones related with fireworks. The peninsular region experiences air-mass movements from central and central-eastern regions, with a high rate of aerosol loading during post-monsoon season (Fig. S1) [42,43], leading to frequent hazy days in recent

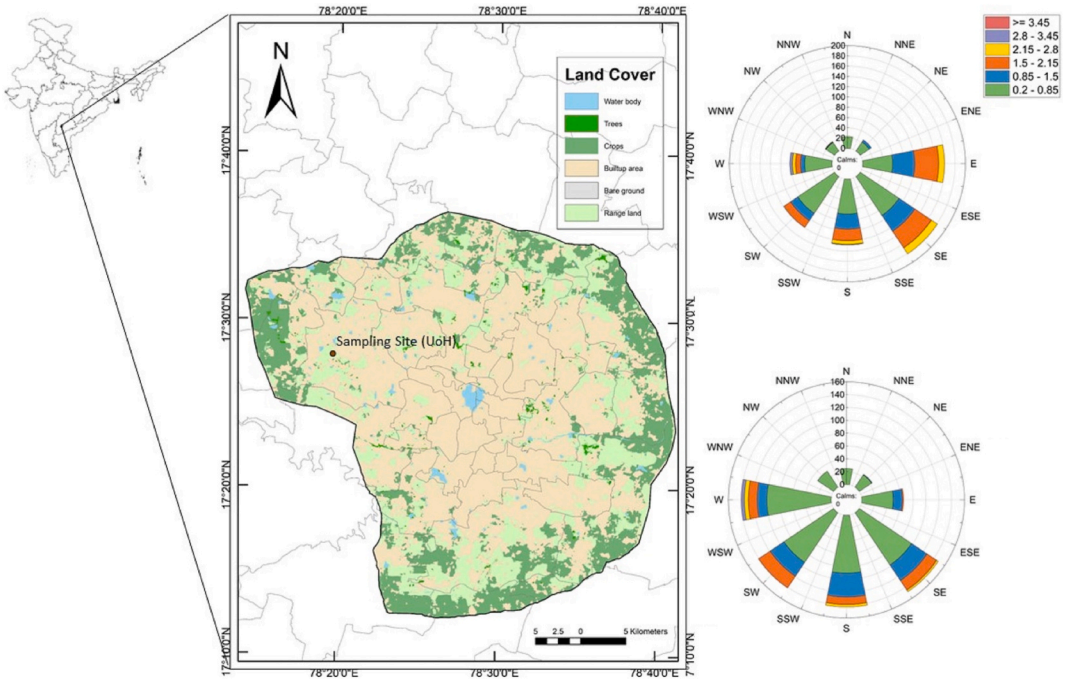

Fig. 1. Geographic location of the (a) study site, CEOAS, UoH, Hyderabad, India and wind speed and direction for Diwali weeks of (b) 2019 and (c) 2020.

years [44]. Several studies have examined the physical properties of aerosols over Hyderabad, which has a complex urban environment with multi-emission sources [45–49]. It is dominated by urban/industrial aerosols throughout the year [46]. The winter and post-monsoonal conditions witness low wind speed with prevalence of well-mixed aerosols from local emissions. The air-mass movements, directed from northern region in post-monsoon season, influence the ambient aerosols over Hyderabad, mainly by

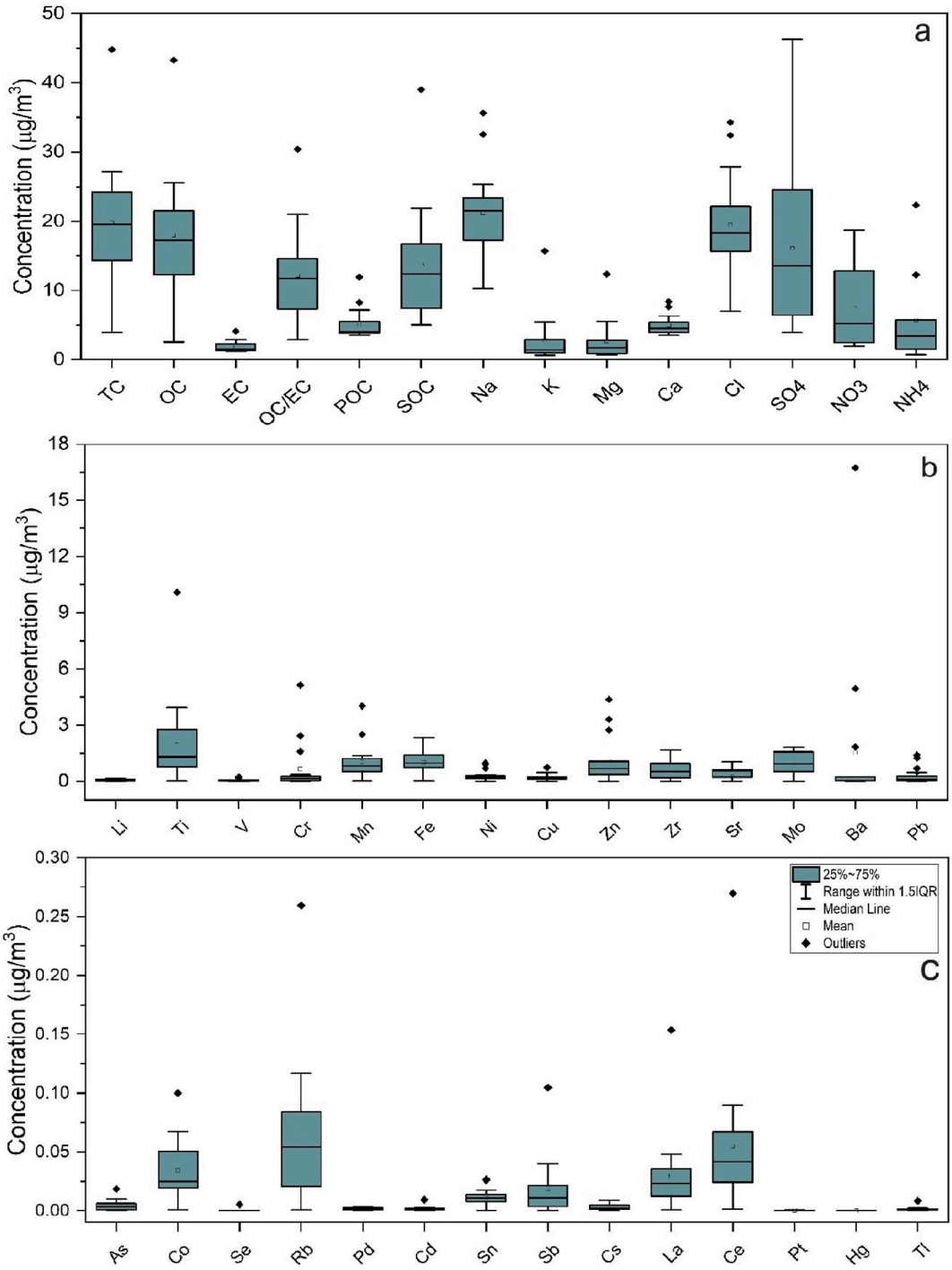

Fig. 2. Box whisker plot of different chemical constituents of PM_{10} in µg/m^3, (a) organic and major ions along with the variability in (b) and (c) elemental species at CEOAS, Hyderabad. Horizontal line within the boxes represents the median; top and the bottom of the shaded area represents the 75thth and 25thth percentile, square inside the shaded region represents the mean, and the upper and the lower limit of the 95thth and 5thth percentiles respectively and the black diamond represents the outliers.

contributing fine-mode particles to it [48]. The crop residue burning in kharif season and the northerly winds usually spread BB aerosols over central and southern India, including Hyderabad [45]. Significant increase in AOD (α) was observed between 2002 and 2008 due to the urbanization, vehicular emissions and growing population in Hyderabad [47]. An average AOD of 0.46 ± 0.18 (0.89 ± 0.19) during post-monsoon and highest fraction (73%) of mixed type of aerosols is reported for Hyderabad [46].

The present study focuses on the atmospheric aerosol chemistry and influence of fireworks in southern city of Hyderabad and attempts to identify the composition of mixed-type aerosols to apportion their sources using chemical compositions, stable carbon isotopes and EPA-PMF model. Particulate matter (size <10 μm) PM_{10} samples over quartz fibre filters for pre-, on and post-Diwali event for two consecutive years of 2019 and 2020 were studied for the chemical compositions and their sources emphasising the effects of post-monsoonal firework activities during the Diwali event in the study area. The objectives were to a) determine the inorganic (trace elements and major ions) and carbonaceous (organic (OC) and elemental carbon (EC)) compositions of PM_{10} b) identify the diagnostic mass closure ratios for fireworks c) apportion the sources using EPA-PMF5.0 receptor model with chemical composition of PM_{10} and stable carbon isotopes of TC and EC. Secondary data such as trace gases and PM concentrations, meteorological data, active fire counts, and air mass trajectories were used to understand the effect and state of the atmosphere during Diwali period.

2. Study area and sampling

The sampling site in the urban city of Hyderabad is located at the Centre for Earth Ocean and Atmospheric Sciences (CEOAS) building in University of Hyderabad (UoH) (Latitude 17° 27′ 55″ Longitude 78° 19′ 37″) and is surrounded by dense vegetation from all sides (Fig. 1) [49]. The city of Hyderabad, in state of Telangana, covers an area of 650 km^2 with the metropolitan population 6.8 million [50]. It lies inland of the southern peninsula and has a subtropical low latitude, semi-arid hot climate. It is characterized by hot (frequent occurrence of temperature >30 °C) and dry (relative humidity (RH) < 50 %) summer, with May being the hottest month of the year [46]. The average annual concentration, provided by Central pollution Control Board (CPCB, 2023) of PM_{10} is 135.1 ± 37.92 μg/m^3.

A high-volume air sampler (Envirotech APM-430) with a flow rate of 0.9–1.0 m^3/min, placed on the roof-top of CEOAS, was used to collect the day and night PM_{10} samples on quartz fibre filter (Whatman; 8 × 12 inches) for the duration of 8 h, pre- (samples collected before Diwali night), on (sample collected on Diwali night i.e. 27thth October 2019 and 14th November 2020) and post-Diwali (samples collected after Diwali night) weeks of the years 2019 and 2020. The day-time sampling was carried out from 9:30 a.m. - 5:30 p.m. Indian Standard Time (IST) and night-time from 10:00 p.m. - 6:00 a.m. IST on pre-desiccated filters, which were pre-combusted at 350 °C for 4 h for the removal of moisture and contaminants. The sampled filters were stored in zip-lock plastic bags and kept at - 20 °C. Gravimetric analysis was conducted before and after the sample collection to obtain the total aerosol loading on the PM_{10} filters. The samples were analysed for WSII (SO_4^{2-}, NO_3^-, Cl^-, Li^+, Na^+, NH_4^+, K^+, Ca^{2+}, Mg^{2+}) using Ion Chromatography (IC), trace metals (As, Ba, Ce, Cs, Li, Ti, V, Cr, Mn, Fe, Co, Ni, Cu, Zn, Se, Rb, Zr, Sr, Mo, Pd, Cd, Sn, Sb, La, Pt, Hg, Tl, Pb) by High-Resolution Inductively Coupled Plasma Mass Spectrometer (HR-ICP-MS) and stable isotopic composition of TC and EC by Isotope Ratio Mass Spectrometer (IRMS). The variations of the measured chemical species are mentioned in Fig. 2.

3. Materials and methods

3.1. Analytical techniques

3.1.1. Water soluble inorganic ions using Ion Chromatography

A 9 cm^2 filter section was cut and soaked in 30 mL milli-Q water (resistivity >18.1 MΩ) for 12 h in pre-cleaned borosilicate test tubes to ensure maximum solubility. Following ultrasonication (40 min, maintained at 22 °C), the soaked samples were filtered to remove the suspended particles [51,52]. A Dionex ICS-90 and ICS-2500 ion chromatograph was used to measure the cations and anions, respectively, in the filtrate. A CS-17 column was used for cation separation with 6 mM (0.38 mL) methane-sulfonic acid (CH_4O_3S) as eluent. A mixed standard of Li^+, Na^+, K^+, Mg^{2+} and Ca^{2+} was prepared in accordance with the approximate sample values to calibrate the instrument. The anions were separated using Dionex™ IonPac AS-14A (carbon eluent anion exchange column) with 0.8 N sodium carbonate (Na_2CO_3) and sodium bicarbonate ($NaHCO_3$) as eluent. Sulphuric acid (H_2SO_4) was used as regenerant, and a mixed standard of F^-, Cl^-, Br^-, NO_3^-, SO_4^{2-} was prepared in the required proportions from the Merck, Germany standards [53] for the calibration of anions over the IC. The CO_3^{2-} and HCO_3^- form eluent for the analytical procedure adopted for IC, hence were not measured for the present study. The measurement (standards and repeated samples) had a precision of ±0.1 % of its total value within the same sequence, and the samples repeated between different sequences had the reproducibility of ±0.1 %. The detection limit for different ions was about 0.1 mg/l. The coefficient of variation for the repeat samples was observed to be 2.2 %.

3.1.2. Trace and rare earth elements (REE) analyses using HR-ICP-MS

For the analysis of heavy, trace and rare earth elements (REE), a section of 15 cm^2 (5 cm × 3 cm) was cut and digested in HDPE Teflon vessels with an acid mixture of HF (0.5 mL) + HNO_3 (1.5 mL) for 4-h on a hot plate. To ensure the complete digestion of sample, the temperature was set within the range of 90–120 °C. Later, 2.5 mL of $HClO_4$ was added to the clear solution and kept for open digestion at 220–240 °C for another 4 h, till the complete evaporation of acid mixture. The residue obtained was dissolved in 6 N HNO_3 and filtered [52,54,55]. The trace and REE metals (Li, Ti, V, Cr, Mn, Fe, Co, Ni, Cu, Zn, As, Se, Rb, Zr, Sr, Mo, Pd, Cd, Sn, Sb, Cs, Ba, La, Ce, Pt, Hg, Tl, Pb) in the sample solution were analysed using the double-focusing, single-collector High-Resolution Inductive Coupled Plasma Mass Spectrometer (HR-ICP-MS) (AttoM® Nu instrument, UK) at Council of Scientific and Industrial Research - National

Geophysical Research Institute (CSIR-NGRI), Hyderabad. The sample introduction consisted of a standard Meinhard® nebulizer with a cyclonic spray chamber, housed in the Peltier cooling system. Silicon (Si), being the main constituent for filter substrate, was not measured in the PM samples. The samples were analysed for trace and REE using ^{129}Xe as an internal standard [56,57]. Geo-chemical reference materials, SO-1, SO-2, SO-3 and SO-4 (CANMET, Canada) were used as external matrix matching standard to evaluate the accuracy and precision. The precisions of <2 % relative standard deviation (RSD) were obtained for majority of elements with comparable accuracy.

3.1.3. Stable carbon isotope ratios of TC and EC using IRMS

In this study, the total organic carbon (TC) is defined as the sum of elemental carbon (EC) and organic carbon (OC) [58,59]. For EC measurements, the HCL fumigated filters were treated following the chemo-thermal oxidation method (CTO – 375) [60,61]. The suitability of the CTO – 375 method and its comparison with other protocols are discussed by several workers [62,63]. The filters were heated at 400 °C in active airflow for 24 h to remove the organic C fractions. The concentrations and isotopic composition ($\delta^{13}C$) of TC and EC were measured using an elemental analyzer; EA (Flash 2000; Thermo Fisher Scientific, Germany) connected to an Isotope Ratio Mass Spectrometer; IRMS (Delta V, Thermo Fisher Scientific, Germany). The IAEA cellulose standard (IAEA–CH– 3; $\delta^{13}C = -24.7$ ‰; C contents = 44 %) was used as laboratory standard. The analytical precision for repeat measurements of standards were better than 10 % (for C content) and 0.1 ‰ (for C isotopic composition). The sample preparation and stable isotopic measurements of TC and EC were conducted at Physical Research Laboratory, Ahmedabad. The fraction of PM_{10} was estimated using analytical protocols published elsewhere [34,64,65].

3.2. Estimation of POC, SOC and $\delta^{13}C_{OC}$

3.2.1. Primary and secondary OC in aerosols

Emission sources such as fuel combustion and vehicular exhaust contribute to the primary OC (POC), while the formation of secondary OC (SOC) includes chemical reactions of semi and non-volatile OCs [66]. EC is considered as a good tracer for carbonaceous aerosols emitted from primary combustion [67]. Linear fit between carbon monoxide and observations of OC and EC have been used to estimate the primary OC/EC [68]. As the concentrations of OC and EC depend on seasonal variations, the minimum value of OC/EC ratios in each season is suggested for the estimation of POC [69]. Determining SOC and POC by direct measurements is difficult, due to challenging separation methods [70,71]. The source composition of EC and POC are similar for the sampling period, thus, EC can be used as a proxy for their estimation [68]. To compute POC and SOC by EC tracer methods, certain assumptions are made, a) SOC is negligible in the sample when OC/EC is minimum for a particular season, b) spatial and temporal variation of chemical constituents and their emission sources in POC and SOC are nearly constant, and c) contribution from non-combustion POC and semi-volatile OC are low compared with non-volatile organic species. Therefore, POC (Eq. (1)) and SOC (Eq. (2)) are,

$$[\mathrm{POC}] = (\mathrm{OC/EC})_{\mathrm{min}} \times [\mathrm{EC}] + c \tag{1}$$

$$[\mathrm{SOC}] = [\mathrm{OC}]_{\mathrm{measured}} - [\mathrm{POC}] \tag{2}$$

where $(OC/EC)_{min}$ is the minimum value of OC/EC ratio in a particular season and, c is assumed to be zero, as the POC from non-combustion sources (primary biogenic sources) is considered negligible and $[OC]_{measured}$ is the measured OC concentration [72]. These assumptions make the estimation of POC susceptible to uncertainties [73,74]. The uncertainties associated with sample collection accounts to be minor [75–77]. [74] compared EC-tracer, SOA-tracer, PMF-chemical data, PMF-offline AMS and PMF-ACSM and suggested an overall low relative uncertainties among other methods. It was also suggested that the PMF approaches were unable to capture the SOC due to BB [73]. proposed a more robust approach for the estimation of SOC, assuming all least correlation between measured EC and estimated SOC, but a significant underestimation of SOC was observed during high BB conditions [73]. Soluble fraction of K+ is commonly used as tracer for BB [78] and in firecrackers as it is used as oxidizers [40]. K and OC are good markers for biomass combustion, which are commonly evident during firework emissions and are considered as indirect sources for it [79,80]. Biomass burning and Diwali fireworks also observe high contribution of m/z 60, m/z 43 and m/z 44, suggesting similar source contribution for both [81]. Anthropogenic fireworks and BB emissions causing smog conditions also show increase in CNC and O_3 [20] along with SO_2, NOx, $\alpha > 1$, high turbidity coefficient, AOD and BC [27]. Therefore, the present study adopted the EC tracer method, as emissions during Diwali are considered similar to a BB event.

3.2.2. Estimation of the isotopic composition of OC from TC and EC

The estimation of $\delta^{13}C_{OC}$, based on isotopic mass balance, was done using the measured compositions of $\delta^{13}C_{TC}$ and $\delta^{13}C_{EC}$ (Eq. (3)).

$$\delta^{13}C_{OC} \text{ x } OC = \delta^{13}C_{TC} \text{ x } TC \; - \; \delta^{13}C_{EC} \text{ x } EC \tag{3}$$

3.3. Miller-Tans analysis

To identify the source isotopic composition, the relationship between $\delta^{13}C$ and the reciprocal of TC concentration after [82] was followed, where $\delta^{13}C$ value and the background concentration of TC can remain unknown, but should be nearly uniform with time [83]. When the TC concentration is zero, the y-axis would be infinite, limiting the applicability of the method. The slope of correlation

between the products of $\delta^{13}C_{TC}$ and TC with TC (Fig. 3a) provides the major sources. The advantage of Miller-Tans plot (Fig. 3c–f) is that the background values of TC and $\delta^{13}C$ need not be constant. It is also useful in calculating the end member, when radiometric isotopic measurements are unavailable [84].

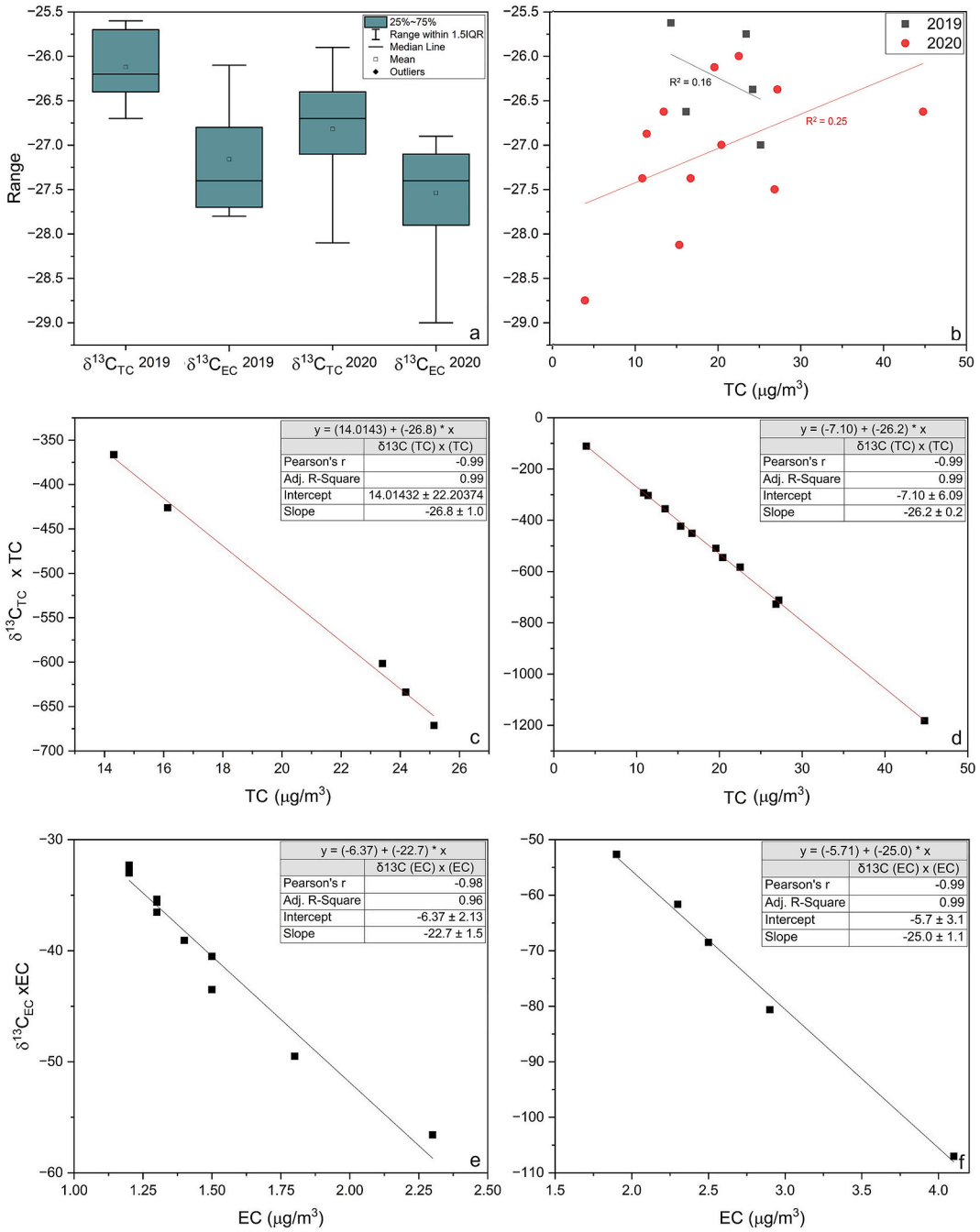

Fig. 3. Box whisker plot of stable carbon isotopic compositions of $\delta^{13}C_{TC}$ (a) and $\delta^{13}C_{EC}$ (b) in PM_{10}, at CEOAS, UoH, Hyderabad. Horizontal line within the boxes represents the median; top and the bottom of the shaded area represents the 75thth and 25thth percentile, square inside the shaded region represents the mean, and the upper and the lower limit of the 95thth and 5thth percentiles, respectively. The black diamond represents the outliers. Correlation between $\delta^{13}C_{TC}$ vs TC ($p < 0.05$), Miller-Tans plot for (c) 2019 $\delta^{13}C_{TC}$ and (d) 2020 $\delta^{13}C_{TC}$ and for (e) 2019 $\delta^{13}C_{EC}$ and (f) 2020 $\delta^{13}C_{EC}$ for Diwali week.

3.4. EPA5.0 positive matrix factorization (PMF) model

The EPA5.0 PMF model attempts to best express the covariance of the multivariate input data. It allows users to down-weight any species concentration based on signal-to-noise ratio (S/N), while ascertaining a prior knowledge of the sampling/analytical errors to calculate the uncertainties (U.S. EPA, 2014). S/N < 0.5 is considered bad (not used for further analysis), $0.5 <$ S/N < 1 weak and S/N > 1 good in the model, based on the analytical extraction efficiency [85]. The method detection limit (MDL) was calculated by

$$\mathrm{MDL} = 3 \text{ x } \sigma \text{ x } s \tag{4}$$

where σ is the standard deviation of the repeated blank during the analysis and s is the slope of the calibration curve [86]. The estimation of uncertainty associated with the analysed chemical constituents is given by

$$Uncertainty = \sqrt{(Error\ fraction \times concentration)^2 + (0.5 \times MDL)^2} \quad \text{Eq. 5}$$

The error fraction is calculated using the standard deviation of samples divided by square root of number of analyses [86]. To best estimate the number of factors with minimum error for small sample sizes, an optimisation between number of factors and block size was attained. The concordance of Q(true) and Q(robust) was achieved to identify the number of factors [87]. The principal component analysis (PCA) was also run to obtain the number of principal components with a cut-off Eigen value of 1. Eight principal components

Table 1
Concentration of organic and inorganic (elemental and major ions) species for 2019 and 2020 in μg/m^3 along with total concentrations of elemental, ionic and carbonaceous content in the samples.

Constituents of PM_{10}	2019			2020		
	Pre-Diwali	Diwali night	post Diwali	Pre Diwali	Diwali Night	post Diwali
PM_{10} sample loading	97.1	252.5	113.09	123.78	166.94	114.23
TC	24.19	25.14	17.95	22.42	20.41	15.20
OC	20.1	22.6	15.6	21.1	18.9	8.5
EC	4.1	2.5	2.37	1.37	1.5	1.55
Na^+	25.29	32.52	21.69	1.64	21.12	20.62
K^+	1.13	31.22	2.39	1.64	15.68	1.81
Mg^{2+}	1.51	5.51	1.78	3.02	5.03	1.8
Ca^{2+}	3.8	4.09	4.91	4.85	5.08	5.53
NH_4^+	–	–	4.60	9.64	3.92	1.84
Cl^-	22.22	27.86	18.98	18.93	15.46	18.92
SO_4^{2-}	–	46.3	18.49	12.76	27.28	9.73
NO_3^-	1.96	13.31	–	8.49	10.37	4.81
Ti	1.13	2.67	2.17	2.21	3.93	1.74
V	0.04	0.09	0.06	0.05	0.09	0.08
Cr	0.03	0.15	0.17	1.03	0.25	0.68
Mn	0.52	1.23	1.00	1.05	2.51	0.79
Fe	0.71	1.88	1.10	0.71	2.35	1.00
Ni	0.21	0.31	0.22	0.27	0.69	0.36
Cu	0.11	0.38	0.20	0.22	0.46	0.16
Zn	0.53	0.88	0.80	1.27	1.09	1.07
Zr	0.35	0.95	0.64	0.40	1.66	0.75
Sr	0.23	0.61	0.48	0.40	0.54	0.49
Mo	0.64	1.66	1.37	0.59	1.81	0.81
Rb	0.03	0.09	0.06	0.06	0.11	0.05
Ba	0.06	16.75	0.71	0.06	4.95	0.49
Pb	0.11	1.26	0.19	0.29	0.68	0.08
La	0.01	0.03	0.02	0.04	0.05	0.02
Ce	0.02	0.05	0.04	0.06	0.09	0.05
Sn	0.01	0.03	0.02	0.01	0.02	0.01
Sb	0.01	0.10	0.02	0.02	0.03	0.01
Co	0.02	0.04	0.04	0.03	0.06	0.03
Li	0.05	0.12	0.1	0.04	0.10	0.04
Pd	0.0007	0.003	0.0013	0.0012	0.0031	0.0015
Cd	0.001	0.001	0.001	0.002	0.002	0.0001
As	0.0027	0.01	0.003	0.003	0.005	0.006
Se	0.0001	0.0005	0.0002	0.0001	0.0002	0.0014
Cs	0.0019	0.0048	0.0039	0.0022	0.0052	0.0019
Pt	0.0002	0.0005	0.0003	0.0001	0.0003	0.0002
Tl	0.0005	0.0017	0.0009	0.0016	0.0021	0.0006
Total Metals	4.84	29.31	9.4	8.8	21.5	8.69
Total Trace Metals	0.13	0.40	0.25	0.21	0.37	0.17
Total Cation	31.74	47.34	35.4	38.4	50.8	31.6
Total Anion	24.2	87.48	37.5	40.2	53.1	33.5
Total Carbon	24.19	25.14	17.95	22.42	20.41	13.88

were identified. 600 EPA-PMF model runs were carried out, and the bootstrap (BS) analysis showed less than 2 % of unmapped cases. This was achieved to find the balance between the selection of number of factors and block size. 8 source factors were identified based on their marker species, corroborating the PCA. The BS and displacement (DISP) were run to estimate the uncertainties associated with the output factor profiles [86]. Out of 600 runs, 11 were unmapped, less than 6 % of runs showed mixing among different factors, and for less than 5 % of the factor profiles, the swap was observed in DISP run, exhibiting reliability of the data [87,88].

Different chemical species have been used to show the factor contribution for various sources. The species contribution towards each factor was quantified in terms of the percentage of factor total (% FT: concentration of species of interest as a fraction of total factor concentration) and the percentage of species sum (% SS: ratio of the concentration of species of interest in the factor of interest to the total species concentration across all factors) [86].

Pearson's correlation among all parameters was performed using OriginPro with significance ($P < 0.05$). Pairwise comparisons of the concentrations of each variable for 2019 and 2020 Diwali periods were performed using Welch's *t*-test, which is widely used for unequal sample sizes, and for data that are not normally distributed and for variances, that are not equal. There was no significant difference between both years except EC and OC/EC. Therefore, one EPA5.0 PMF model simulation containing both year datasets was run.

4. Results and discussion

The Chemical and isotopic compositions of the aerosols from Hyderabad are presented in Tables 1 and 2 respectively. These revealed mixed, complex emission sources such as sea spray, biomass burning, and fireworks. Understanding the properties and variations amongst these offers insights into their contribution.

4.1. AOD and α

The monthly average AOD550nm for October (November) 2019 was 0.12 (0.14), and for 2020, it was 0.4 (0.34), while the α was observed to be 1.4 (1.6) and 1.4 (1.5), respectively (Fig. S2). For Hyderabad [46], observed the higher frequency for AOD and α to be 0.5 ± 0.2 (range of 0.3–0.5) and 0.9 ± 0.2 during post-monsoon and moderately turbid conditions with mixed type of both fine and coarser aerosols. $\alpha > 1$ for October and November months showed dominance of finer particulates at sampling location. AOD and BC fraction within atmospheric boundary layer were suggested to be about 80% and 11.8%, respectively during post-monsoon, due to long-range transport of aerosols [48]. On Diwali night, the AOD550nm of 0.5 and 0.6 was observed for 2019 and 2020, with α was 1.3 and 1.5, respectively, suggesting contribution of finer aerosols during Diwali compared to normal conditions. The fire radiative power (FRP) (>50 % confidence) ranged from 0.4 to 4.0 MW and 0.5–10.5 MW, with total number of 42 and 383 events for 2019 and 2020, respectively during the Diwali week in the state of Telangana, India (Fig. S3), suggesting contribution from long-range transport of burning sources at sampling location.

4.2. Variations in PM_{10}

In comparison to other locations in Hyderabad (Fig. S4), the sampling site (UoH) had lowest concentrations of PM and other chemical species such as benzene, toluene, and xylene (Fig. S5). The sampling site is surrounded by vegetation and is less impacted by urbanization. The firework activities at the sampling site were relatively less compared to other populated parts of the city (Fig. S5), which also provided an opportunity to assess the overall ambient air quality and the background condition for Hyderabad during Diwali week. Fig. S5 presents the hourly time series of October and November 2019 and 2020 p.m.$_{10}$ concentration. In general the PM_{10} concentration is higher during October, compared to November over Hyderabad [41]. The time series of CPCB PM_{10} also showed overall concentration to be higher before Diwali week (Fig. S5) following which, there was decline after Diwali due to wet scavenging (Fig. S6). Similar decrease in AOD and FRP (Fig. S3) was also observed for 2019 Diwali week. On Diwali night, the PM10 loading (8-h) obtained on the quartz fibre filters was 212.5 μg/m^3 (167 μg/m^3) for 2019 (2020), suggesting impact of fireworks.

4.3. Ionic constituents

The abundance of major ions in PM_{10} sample loading for 2019 was $SO_4^{2-} > Na^+ > Cl^- > NO_3^- > NH_4^+ > Ca^{2+} > Mg^{2+} > K^+$, while for

Table 2
Average concentrations of TC, EC and OC during Diwali week along with day and night time concentration on the day of Diwali and their isotopic composition for 2019 and 2020 in μg/m^3.

	2019 Diwali week average	2019 Diwali night	2019 Diwali day	2020 Diwali week average	2020 Diwali night	2020 Diwali day
TC	20.63 ± 5.02	25.14	16.14	19.41 ± 9.7	20.41	16.69
$\delta^{13}C_{TC}$	−26.1 ± 0.5	−26.7	−26.4	−26.8 ± 0.7	−26.7	−27
EC	2.74 ± 0.84	2.5	2.9	1.44 ± 0.32	1.5	1.3
$\delta^{13}C_{EC}$	−27.2 ± 0.7	−27.4	−27.8	−27.4 ± 0.7	−29	−27.2
OC	17.89 ± 4.9	22.64	13.24	17.97 ± 9.6	18.91	15.39
$\delta^{13}C_{OC}$	−26.0 ± 0.5	−26.6	−26.1	−26.7 ± 0.7	−26.5	−27

2020 it was $Cl^- > SO_4^{2-} > Na^+ > NO_3^- > K^+ > Ca^{2+} > NH_4^+ > Mg^{2+}$ (Table 1). The average WSIIs concentration for the sampling duration was 67.5 and 72 μg/m^3 for 2019 and 2020 respectively. The anions and cations concentrations on Diwali night were 1.5 (1.3) and 3.6 (1.3) times higher than pre-Diwali for respective years. A study in Bhilai, Chhattisgarh, India also observed similar increase in cations and anions concentrations during Diwali nights [89]. The secondary WSIIs, namely, NH_4^+, NO_3^- and SO_4^{2-} account for about 59.6 μg/m^3 and 41.6 μg/m^3 for respective years on Diwali nights, which were highest for the sampling period (Fig. 2a and Table 1).

For the sampling period, the average TAE/TCE ratios (total anion equivalent/total cation equivalent) (Supplementary data Section 1) were 1.1, while, for both years of Diwali night, these were 1.4 and 1.1, respectively. TAE/TCE ratios (>1) during Diwali week for both years suggest the cation deficiency. This may be due to exclusion of H^+, causing acidic nature of aerosols [90] and can be attributed to the use of firecrackers on Diwali nights [89–91]. A study in Chennai suggested contribution of H_2SO_4 and NH_4HSO_4 along with the NH_4NO_3 and $(NH_4)_2SO_4$ during winter [90].

Typically, the ratio of NH_4^+ and SO_4^{2-} is also used as an indicator of acidity or/and basicity in aerosols [92,93]. The volatility of NO_3^- and NH_4^+ pose challenges in defining the chemical nature of aerosols. Due to these constraints in determining the contribution of basicity by these ions, the input of these from few other sites of southern Indian locations were compared with that of the sampling site in present study. The carbonate (CO_3^{2-}) and bicarbonate (HCO_3^-) contribute to the basicity of the aerosols. Crustal and marine aerosols cause carbonates and bicarbonates enrichment in ambient aerosols [94]. The soluble fractions of CO_3^{2-} and HCO_3^-, react with available Ca^{2+} and Mg^{2+} therefore, their higher concentrations in general, indicate the presence of CO_3^{2-} and HCO_3^- in the aerosols [95]. In the present study, the average concentration of Ca^{2+} and Mg^{2+} were 2.47 ± 2.12 μg/m^3 (2.78 ± 3.23) and 4.53 ± 1.74 μg/m^3 (5.10 ± 1.32) for Diwali period of 2019 (2020), while on Diwali nights, there was a considerable increase in Mg^{2+} in 2019 (5.51 μg/m^3) and 2020 (12.35 μg/m^3), and the Ca^{2+} remained more or less the same for pre-, on and post-Diwali. This could be due to the presence of Mg powder, used as reducing agents in firecrackers [96,97]. [98] has reported high concentration of Mg^{2+}, sourced from firecrackers in Nagpur on Diwali night and, similar was observed in Chinese new year firework celebration [80]. A study over Agra in northern India during normal and hazy conditions showed the concentrations of Ca^{2+} and Mg^{2+} to be below 3.5 ± 1.1 μg/m^3 [99], implying lesser anthropogenic contribution of Mg^{2+}. To understand CO_3^{-2} and HCO_3^- fractions for the sampling site, the concentrations of Ca^{2+} and Mg^{2+} were compared with locations in peninsular India. Lower concentrations of Ca^{2+} (1.6 ± 1.4 μg/m^3) and Mg^{2+} (0.3 ± 0.2 μg/m^3) were observed over Coimbatore during post-monsoon 2014–2016 and the average HCO_3^- concentration was 1.50 ± 1.20 μg/m^3 [100]. In the coastal city of Thiruvananthapuram, the concentrations of Ca^{2+} and Mg^{2+} were 1.7 ± 0.4 μg/m^3 and 1.6 μg/m^3 respectively, while the HCO_3^- concentration ranged from 3.1 to 4.9 μg/m^3 [94]. In general, the lower concentration of Ca^{2+} and Mg^{2+} suggest the lack of soluble fraction (precipitate) of CO_3^- and HCO_3^- [95]. In view of these observations, the HCO_3^- concentration over sampling site was assumed to be low, suggesting slightly acidic nature of aerosols.

4.4. Mass closure and diagnostic ratios

Na can also be contributed from dust [101], apart from sea-salts [102]. Cl^-/Na^+ (1.8) is a common tracer for sea-salts [103]. Sea-salts are important source of cloud condensation nuclei (CCN), due to their hygroscopic nature and large particle sizes, which also allow droplet activation [104,105]. During sampling period, the average Cl^-/Na^+ ratios for 2019 and 2020 were 0.87 (0.84–0.91) and 0.96 (0.44–1.7), respectively. The Cl^-/Na^+ ratio <1 suggests smaller contribution of sea-salt and depletion of Cl^-. A study in Greece observed higher Cl^-/Na^+ ratio of 3.3, suggesting BB contribution to Cl^- [106]. The sampling site is located inland of coast, thus non-sea-salt (nss) sources of Cl^- from incineration and combustion sources would contribute towards the addition of Cl^- in the aerosols [107]. The aging of inland moving sea-salts accompanies Cl^- depletion and its replacement by NO_3^- [108]. Higher concentration of SO_4^{2-} and NO_3^- (Table 1) due to Diwali fireworks and other anthropogenic emissions, with depletion of Cl^- lead to synthesis of $NaNO_2$ and Na_2SO_4 [109,110], which is reflected in the abundances of these ions in the samples. The low Cl^-/Na^+ ratio in the studied samples suggests the reduction of sea-salt aerosols in the urban environment of Hyderabad.

K^+ concentrations at the sampling site showed sharp increase on Diwali nights of 2019 (31.02 μg/m^3) and 2020 (15.68 μg/m^3). When compared to another urban location like Delhi (K^+ = 72.02 μg/m^3 during the day of Diwali) [19,111], these are observed to be quite low. K^+ is an important primary tracer for aerosols from BB and firecracker sources [112]. Being stable alkali metals, K^+ and Na^+ persist longer in the atmosphere, and the K^+/Na^+ ratio helps in identifying the contribution from different emission sources (Na^+ for sea-salt; K^+ for Biomass burning/fireworks) [113][114]. The majority of K^+ originates anthropogenically (BB and other activities) and Na^+ from natural sources (soil and sea-salt) [114,115]. To account for the sources from non-sea-salt, K^+ was corrected using Na^+, considering it as a tracer for sea-salt. In general, the K^+/Na^+ ratio for ambient aerosols varies in the range of 0.03–10 [114]. For sea-salt the K^+/Na^+ ratio is 0.036 [116], while for aerosols originating from incineration processes, it is in the range of 1.2–1.7 [117] and 1.8 [118]. The non-sea-salt K^+ (K^+_{nss}) is obtained by subtracting 0.036*[Na^+] from the [K^+], which is 96.3 and 95% of the total K^+ for respective years. In finer PM, the K^+/Na^+ ratio is suggested to be 0.80 (PM_1) and 0.52 ($PM_{2.5}$) for non-sea-salt sources [119]. In the present study, the average K^+/Na^+ ratio for the sampling duration was observed to be 0.19 (0.14) for 2019 (2020), while on Diwali night, maximum K^+/Na^+ ratio of 0.95 (0.74) was observed for respective years, suggesting contribution from the fireworks. K^+_{nss}/Ca^{2+}_{nss} ratio for Diwali week were 5.65 ± 3.65 (3.75 ± 2.40), indicating higher contribution of K^+_{nss}. For PM > 2 μm, K^+/Ca^{2+} ratio >0.75 for non-sea salt sources is reported [120]. Here, the average K^+/Ca^{2+} of 4.57 (3.35) was observed for 2019 (2020), suggesting impact of firecrackers. A positive correlation between Mg^{2+} and Ca^{2+} (R^2 = 0.65: P < 0.05) indicated major contribution of Mg^{2+} from dust/soil, roadside and construction contributions (Fig. S7).

In the present study, K^+_{nss}/OC was in the range of 0.01–0.21 (0.01–0.10) for 2019 (2020), except on Diwali night, which observed a higher K^+_{nss}/OC ratio of 1.37 (0.79), thus, allowing the ratio to be an indicator for fireworks. Studies in Beijing, Shanghai and Ioannina, Greece observed the K^+/OC of 0.19–0.21 [121], 0.21 [122] and 0.01–0.21 [106], suggesting contribution from open BB. For

non-Diwali nights, similar was observed for the sampling site in the present study for both years. Considering other reported ranges of K^+/OC, the agricultural residue burning [123] and Savanna burning [124] were 0.04–0.13 and 0.08–0.10, respectively. Therefore, this sudden increase in K^+_{nss}/OC at the sampling location during Diwali nights can only be attributed to the emissions contributed from the firecrackers burning.

In Addition, NH_4^+ and SO_4^{2-} showed significant positive correlation with OC, which suggest the increase in secondary inorganic components under turbid atmospheric conditions [106]. PM_{10} vs OC, PM_{10} vs SO_4^{2-} and SO_4^{2-} vs NO_3^- showed positive correlation (R^2 = 0.87, 0.86 and 0.84: $P < 0.05$) (Fig. S7), indicating similar sources of origin. Due to the high concentration of NO_3^-, NH_4^+, Na^+, Cl^- and SO_4^{2-} and the presence of moisture during the 2019 Diwali week, suggest the formation of deliquescent salts such sodium chloride (NaCl), ammonium nitrate (NH_4NO_3) and ammonium sulphate ($(NH_4)_2SO_4$) [106,125,126].

4.5. Metallic contribution during Diwali

The variation in concentrations of different trace metals is shown in Fig. 2b and c. The abundance of metals in PM_{10} samples for 2019 were as follows: Ba > Ti > Fe > Mo > Mn > Zn > Zr > Pb > Sr > Ni > Cu > Cr > Li > V > Rb > Sb > Ce > Co > La > Sn > As > Cs > Pd > Tl > Cd > Pt > Se, while for 2020, these were Ti > Ba > EC > Mn > Fe > Zn > Mo > Zr > Cr > Sr > Ni > Pb > Cu > V > Rb > Ce > Li > Co > La > Sb > Sn > As > Cs > Pd > Tl > Cd > Se > Pt. In the present study, the quantity of several metals such as Li, La, Ce, Sn, Sr, Co, Pd, Cd, As, Se, Cs, Pt, Tl are found to be in trace concentration (Table 1), while the others were comparatively more abundant. The total concentration of trace metals on Diwali night were 0.40 μg/m^3 and 0.37 μg/m^3 for respective years of 2019 and 2020. The percentage contribution of total metals (TM) was 11.71 % and 9.84 %, for respective years to the PM concentration, while for Diwali nights, it was 15.5% (29.3 μg/m^3) and 20.3% (28.78 μg/m^3), respectively. The overall contribution of Ba and Fe were 57.1 % and 23 %, respectively. The contribution of Ba and Fe to the TM were 16.75 (4.95) μg/m^3 and 1.88 (2.35) μg/m^3, respectively for 2019 (2020) on nights of Diwali, which are higher than pre- and post-Diwali, thus confirming firework emissions as a source for these metals. The Fe concentration on Diwali night is reported to be twice higher than normal days [40]. Perchlorate, oxalate and nitrate salts of Ba impart green colour [40] and are used as oxidizers in fireworks for rapid combustion [127]. Fe helps in producing sparks and other elements are also used to provide colour and sparkles [128]. The inclusion of lead oxide (PbO) in pyrotechnics as colouring agent [129] maybe the cause of high contribution of Pb at the sampling site for both years of Diwali nights. Ba, along with Pb, Sb, Sr and Fe increased by 305 (87), 12 (11), 12 (3), 3 (2) and 3 (4) times on night of Diwali, as compared to pre-Diwali of 2019 (2020) and were recognized as metallic tracers for firework emissions in the present study. Few amongst these have also been mentioned as tracers by other workers [40,128]. A significant correlation of 0.72, 0.58, 0.51, 0.44 and 0.38 ($P < 0.05$) for PM_{10}-Ba, PM_{10}-Pb, PM_{10}-Sn, PM_{10}-Fe, PM_{10}-As (Fig. S7) were observed. During the sampling period of Diwali week, these elements show contributions majorly from the firecrackers.

For the sampling duration, the sources of La, Ce, V and Rb were identified using La/Ce, La/V and V/Rb. La/Ce greater than 1 indicates the contribution of fluid catalytic cracking (FCC) emissions from oil refinery [130], while the values between 0.4 and 0.6 indicate contribution from the upper continental crust (UCC), mainly minerals, soils and uncontaminated rocks [131]. In the present study, the La/Ce ratio was <1(Fig. 4), indicating a source other than oil refinery. Throughout the sampling period, La/V ratio was <0.15, which suggested the contribution to be different from oil combustion [130]. The soluble fraction of Rb was attributed to BB [132,133], whereas insoluble fraction was attributed to sea-salt and soil dust resuspension [133]. Rb in ambient aerosols is an indicator of natural sources such as crustal minerals.

4.6. Carbonaceous constituents and their climatic effects

The OC and EC concentrations during 2019 (2020) ranged from 12.0 to 22.6 (3.9–44.8) μg/m^3, and 1.9 to 4.1 (1.2–2.3) μg/m^3,

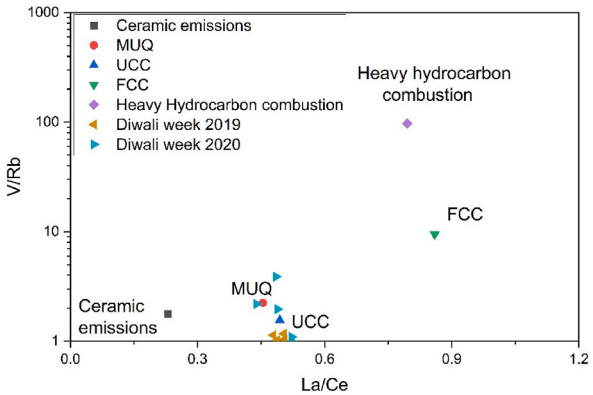

Fig. 4. Scatter plot between La/Ce and V/Rb and its association with crustal rocks. Upper crustal compositions (UCC): magenta triangle and MUQ is standard for unconsolidated argillaceous sedimentary rocks: red circle, heavy hydrocarbon combustion: orange diamond, fluid catalytic cracking units (FCC): gray down arrow, ceramic emissions: light gray square, Diwali week 2019: blue triangles and Diwali week 2020: cyan triangles [174, 175]. (For interpretation of the references to colour in this figure legend, the reader is referred to the Web version of this article.)

while on nights of Diwali, these were 22.6 (18.9) μg/m^3, and 2.5 (1.5) μg/m^3 respectively. During Diwali 2015, a study in Delhi observed an average concentration of OC and EC of 99.2 μg/m^3 and 24.3 μg/m^3, respectively [134] reported higher contribution of EC on Diwali night. These were several times higher than those over Hyderabad. On Diwali nights, the OC/EC for the sampling location was observed to be 10.2 (13.9) for 2019 (2020), while for Diwali week, its average values were 8.1 and 12.0 for 2019 and 2020, respectively. The concentration of OC predominated over EC in Hyderabad and the high OC/EC ratios, ranging from 5.7 to 12.3 (2.9–21) for 2019 (2020), indicated contribution from secondary organic aerosols (SOA). In the peninsular India, OC/EC ratio is reported to be 5.7 and 5.0 for Coimbatore [100] and Thiruvananthapuram [135], respectively, owing to BB emissions and SOA formation. For Hyderabad as well, it was observed to be the same. Coastal city of Chennai observed OC/EC of 1.5 [136], suggesting the dominance of biofuel/biomass burning during winter. These were formed due to chemical reactions involving VOCs and other precursor gases [38,137].

The average estimated POC and SOC for Diwali week were 7.9 ± 2.5 (4.2 ± 0.9) μg/m^3 and 10.0 ± 5.4 μg/m^3 (15.2 ± 9.5) μg/m^3 for 2019 (2020), while for Diwali night, the estimated SOC was 15.6 (14.7) μg/m^3 for 2019 (2020). Higher fraction of SOC can be attributed to the co-existence of localized, long-range transport and festive event [138]. In comparison to 2020, high average POC and SOC concentrations were observed for 2019, which were also reflected in increased mass loading of PM_{10}. The significant positive correlation for EC vs POC and SOC vs OC was 0.97; ($P < 0.05$) (Fig. S7), which suggested similar sources and formation mechanisms [87].

To determine the cooling and warming effects of combustion aerosols on the atmosphere, the effective carbon ratio (ECR = SOC/(POC+EC)) is assessed [87,134]. Low ECR values point to the existence of carbonaceous aerosols that absorb light and the warming effect of combustion sources [87,134]. ECR ranged from 0.5 to 2.2 (1.1–6.7) for 2019 (2020) Diwali weeks. The high SOC and ECR at the sampling site implied a decrease in light-absorbing carbonaceous aerosols, which would have caused a cooling impact. Studies in Delhi during the post-monsoon also observed similar increase in SOC and ECR and therefore, revealed presence of light scattering aerosols causing cooling effect [25,139]. Urban cities such as Hyderabad and Delhi exhibit similar light scattering aerosols presence during post-monsoon period. Conversely, Pune [87], Mount Lu in south China [140], and five European cities [141] observed warming effect of aerosols.

4.7. $\delta^{13}C$ of carbonaceous aerosols (TC and EC) and associated transformation processes

Both OC and EC are emitted from the incomplete combustion processes such as BB (crop residue, wood, and forest fires) and fossil fuels (petrol, diesel and coal) [142]. EC is as primary constituent, while OC can also form from secondary processes (aging and oxidation of different VOCs) [143]. OC and EC exhibit different $\delta^{13}C$ signatures from the same combustion sources [63]. Due to the inert chemical nature of EC, it retains the source emission signatures [63,142,144], while the OC is affected by other sources and atmospheric processes [145]. $\delta^{13}C$ of EC helps in distinguishing the combustion sources [142], while the $\delta^{13}C$ of OC provides information on the aging process and chemical transformation following emissions from a common source.

$\delta^{13}C_{TC}$ of the aerosol samples from Hyderabad during Diwali weeks of 2019 and 2020 were in the range of −26.7 to −25.6; −26.1 ± 0.5 ‰ and −28.1 to −25.9; −26.8 ± 0.7‰, respectively (Table 2). The isotopic ratios closely resemble the diesel and C_3 plant burning [32,36,146]. The average $\delta^{13}C_{TC}$ at the sampling site was slightly depleted by −0.6 ‰ in 2020, compared to 2019. $\delta^{13}C_{TC}$ for firecrackers powder is reported to be −21.5 ± 1.6 ‰ [147]. Generally, $\delta^{13}C$ of C_3 plants burning emissions range from −30 to −27 ‰, while the average $\delta^{13}C$ of diesel burning emissions is −26 ± 1 [32]. The forest fire derived airborne PM is in the range of −27 to −23 ‰ [36,146,148]. Studies at Sinhagad, west-India, observed $\delta^{13}C_{TC}$ and $\delta^{13}C_{WSOC}$ of −22.5 ‰ and −21‰ [34] for post-monsoon season, with annual average of −22.57 ± 0.68 [64]. Urban Indian cities like Ahmedabad and Jodhpur showed the $\delta^{13}C_{TC}$ values during summer to be −31 and −29.6 ‰, which were attributed to SOA and primary biological aerosols [149]. In the urban environment of Hyderabad, $\delta^{13}C_{TC}$ during post-monsoon Diwali weeks samples were enriched compared to Ahmedabad and Jodhpur, suggesting meagre contribution from biogenic aerosols. Another study in the capital city of Delhi witnessed higher average PM concentrations compared to Hyderabad, along with the $\delta^{13}C_{TC}$ for Diwali night 2016 (a post-monsoon smog condition) of −25.5 ‰ [147]. Here, the $\delta^{13}C_{TC}$ on the nights of Diwali were −26.7 and −27.0 ‰ for 2019 and 2020, respectively. Depletion of $\delta^{13}C_{TC}$ at the sampling site was observed during Diwali week, when compared to an urban environment like Delhi [147]. Although high TC was observed for Diwali night samples for both years at the sampling site, $\delta^{13}C_{TC}$ values did not show considerable change, indicating meagre influence of firecrackers. The sampling site was observed to be more influenced by fossil fuel combustion/BB, which produce high carbonaceous matter and VOCs [150]. There was in increase in toluene during Diwali week suggesting (Fig. S5), suggesting higher contribution of SOA [38], thus corroborating the significance of toluene in formation of SOA.

Overall, the isotopic values in carbonaceous aerosols of ambient particulate matter between pre-Diwali and post-Diwali for both the years did not show any considerable difference. The ambient OC is not chemically stable [63], thus source apportionment is complicated by isotope fractionation, along with OC aging and biogenic SOA formation [137]. Fig. 3b shows the weak positive correlation between TC and $\delta^{13}C_{TC}$ correlation ($R^2 = 0.25$; $P < 0.05$), which suggests that the atmospheric state was not significantly different from the normal conditions. It further corroborates the inference that $\delta^{13}C$ values during Diwali were mainly due to mixing of emissions from C_3 plant burning and liquid fuel combustion, and is consistent with the previously documented work in Goa [32]. Air mass trajectories during sampling period, along with the FRP (Fig. S3) suggests north-westerly winds and increased biomass burning activity in the surrounding regions of Hyderabad.

Combustion processes (coal combustion, BB and vehicular emission) and pyrolysis are primary sources of EC [63]. EC constitutes light absorbing aerosols [151]. Its inert nature helps in identifying the source composition [63]. For the present study, $\delta^{13}C_{EC}$ ranged from −27.8 to −26.1; −27.2 ± 0.7 ‰ and −29.0 to −26.4; −27.4 ± 0.7 ‰ for Diwali weeks of 2019 and 2020, respectively with no

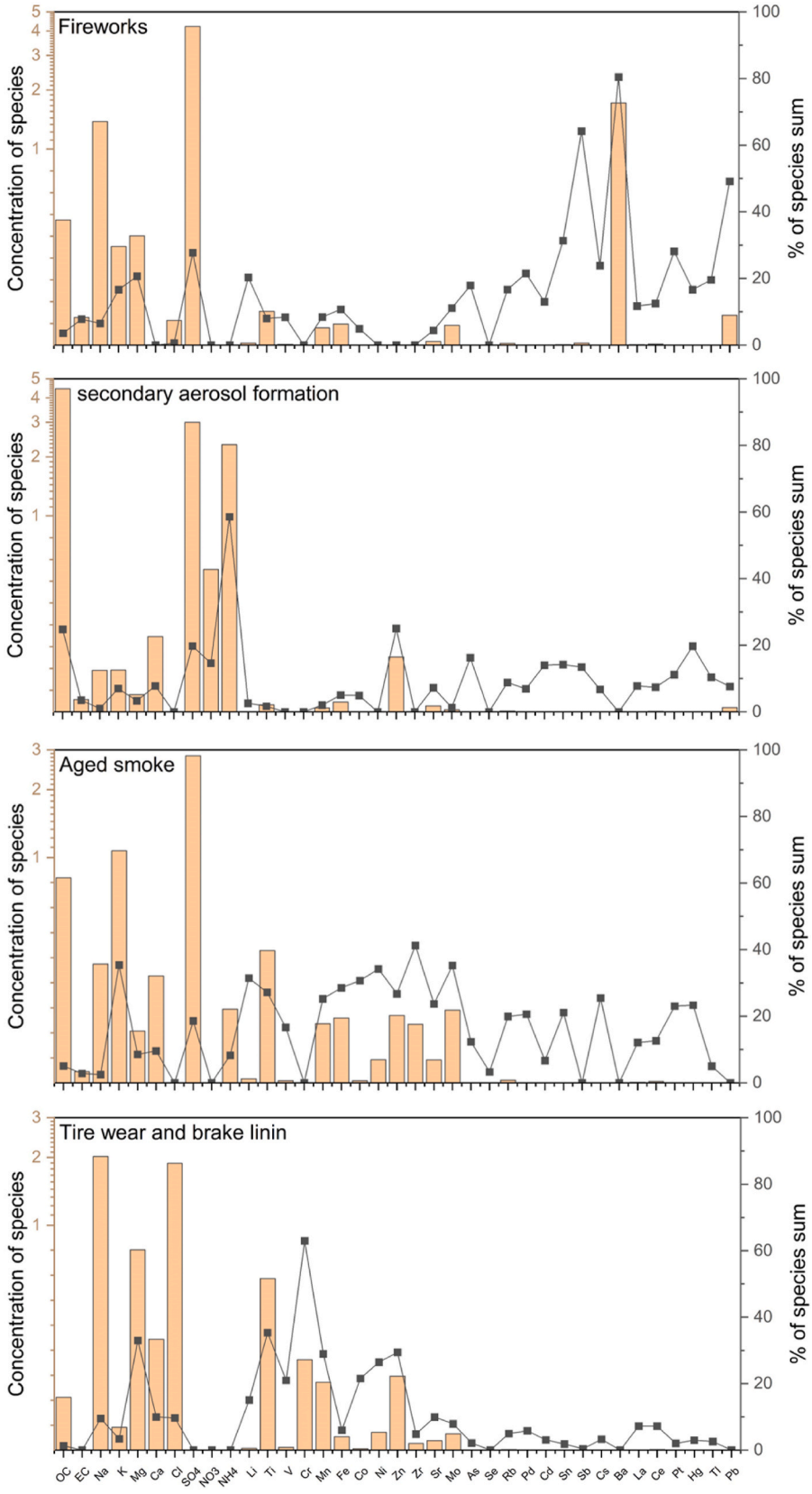
Fireworks
secondary aerosol formation
Aged smoke
Tire wear and brake linin
Concentration of species
% of species sum
OC
EC
Na
K
Mg
Ca
Cl
SO4
NO3
NH4
Li
Ti
V
Cr
Mn
Fe
Co
Ni
Zn
Zr
Sr
Mo
As
Se
Rb
Pd
Cd
Sn
Sb
Cs
Ba
La
Ce
Pt
Hg
Tl
Pb

Fig. 5. (a) 8 factors were resolved by EPA5.0 PMF model analysis and were identified as fireworks, secondary aerosols formation, industrial and aged smoke, vehicular emission (brake linings, tire wear). (b) 8 factors were resolved by EPA5.0 PMF model analysis and were identified as crustal rock dusts, solid fuel/coal combustion, residue and waste burning processes, marine/road side dust.

considerable difference (Table 2). $\delta^{13}C_{EC}$ for Diwali night samples were −27.8 and −29.0 ‰ for 2019 and 2020 respectively, which were more depleted in $\delta^{13}C_{EC}$ as compared to pre- and post-Diwali samples. The standard deviation of $\delta^{13}C_{EC}$ for the sampling duration was 0.7 ‰ (1.0 ‰) for 2019 (2020) respectively, suggesting no considerable variation in sources during day and night time.

To the best of authors knowledge, $\delta^{13}C_{EC}$ has not been reported in India. Apart from the present study, South Asian Pollution Experiment 2016 field campaign (SAPOEX-16) observed $\delta^{13}C_{BC}$ at Maldives (−25.4 ± 0.2 ‰) and Bangladesh (−27.6 ± 0.2 ‰) climate observatories, and suggested transport from IGP and Arabian sea, respectively, with influence of C_3 coal, liquid fuel combustion [144]. A study over Xi'an, China from 2008 to 2009 showed the average annual $\delta^{13}C_{EC}$ of −24.9 ± 1.1 ‰ (−26.5 to −22.8 ‰), while during autumn, it was −25.1 ± 0.7 ‰ [145], suggesting major contribution from C_3 plants, liquid fossil fuel and coal combustion. In C_3 plant burning (woods) and traffic emissions, the $\delta^{13}C$ for EC shows more depleted values compared to TC, while it was enriched for coal combustion [63]. The $\delta^{13}C$ for EC for coal combustion is −23.3 ‰ [146], which is highly enriched compared to present study. These indicate that overall emission during the sampling period for Hyderabad had no considerable influence of coal combustion.

A weak positive correlation ($R^2 = 0.19$; $P < 0.05$) between $\delta^{13}C_{EC}$ and $\delta^{13}C_{TC}$ was observed for 2020, while no significant correlation was found for the same in 2019, a study in Japan suggested observed similar weak positive correlation suggesting different sources of emissions [146]. Similar was observed for estimated $\delta^{13}C_{OC}$. In general, $\delta^{13}C$ of TC, EC and OC in different sources get depleted in similar order (C_4 plants burning > coal combustion > traffic emissions > C_3 plant burning) with small variation among them [63]. The slope values of Miller-Tans plot for TC, OC and EC were −26.8, −26.8 and −25 ‰ (with $R^2 = 0.99$; $P < 0.05$) for 2019, while these were −26.2, −26.2 and −22.7 ‰ for 2020, respectively (Fig. 3c and f). The Miller-Tans analysis suggests the end members to be diesel and C_3 plant burning for TC and OC; while for EC, the end members are C_3 plant burning, liquid fuel and slight contribution from coal combustion. For both years Diwali weeks, TC was enriched in ^{13}C compared to EC except for 2 samples of post-Diwali 2020. During post-Diwali 2020, high OC/EC ratio along with depleted $\delta^{13}C_{OC}$ compared to $\delta^{13}C_{EC}$, suggests the formation of secondary aerosols formation (SOA). Due to the surrounding flora around the sampling site, biogenic contribution was expected in the OC fraction, but the $\delta^{13}C$ of TC and OC in the studied samples do not show influence of biogenic sources. In general, the sampling site observed enrichment of $\delta^{13}C$ of OC compared to EC ($\delta^{13}C_{OC} > \delta^{13}C_{EC}$), suggesting dominance of photochemical aging of aerosols during long range transport [37,38]. It is reported that South-Asian region exhibits the aging of OC from long range transport [142, 152]. Similar was observed for Sinhagad, western India [34,64]. During pre-Diwali 2019 and post-Diwali 2020, OC is depleted compared to EC ($\delta^{13}C_{EC} > \delta^{13}C_{OC}$), suggesting SOA formation. Increase in toluene concentration (Fig. S5) during Diwali week also suggests contribution of fresh SOA formation. As oxidants react with precursor ^{12}C during SOA formation, ^{13}C undergo depletion compared to precursors during photochemical oxidation [38,137].

4.8. Source apportionment of PM_{10}

The observed chemical concentrations (OC, EC, major ions, and trace metals and REE) were assessed for their sources using EPA-PMF and stable isotopic composition of TC and EC. A compilation of studies utilising the information of trace elements and major ions for the source apportionment of PM and identification of certain species as marker are presented in Table S2.

4.8.1. Eight factored sources from EPA5.0 PMF model

4.8.1.1. Factor-1: fireworks. There are specific markers, which originate from the firework emissions. Typically, sulphur is used as fuel in firecrackers [5,153], whereas K and perchlorate salts of Ba are used as oxidizers for rapid combustion [154]. Additionally, K is also present as $KClO_3$ or KNO_3. Pb is mainly employed as colouring agent in firecrackers [11,155]. The combustion of firecrackers also releases OC.

In the PMF model for the present study, the percentage contribution of species sum (SS %) of Ba (80.45 %), K^+ (16.3 %), Li (20.3 %), Sb (64.2 %) and Pb (49.2 %) have been considered for fireworks, and are assigned as Factor-1 (Fig. 5a). Total concentration of species (CS) of Factor-1 was observed to be 10 μg/m^3 (9 %) (Fig. 6), whereas the total concentration of metals to the Factor-1 was 2.42 μg/m^3. The % factor contribution of TM to the Factor-1 on Diwali night sample was 61.9 % (20 %) of 2019 (2020). The concentration of SO_4^{2-}, Ba, OC, and K^+ contributing to the total PM were 4.21 μg/m^3, 1.72 μg/m^3, 0.64 μg/m^3 and 0.50 μg/m^3. The percentage contribution of SO_4^{2-}, Ba, OC, and K^+ were 42.2, 17.25, 6.4 and 5% to the total PM. Therefore, K^+, Ba, SO_4^{2-} and OC were considered as tracers for Diwali fireworks.

4.8.1.2. Factor-2: secondary aerosols (SA). Secondary aerosols are formed through chemical reactions in the atmosphere involving primary pollutants such as NOx, SO_2 and OCs. These are mainly emitted from the industries and vehicles. In the present study, the total concentration of SA formation for the sampling duration was 11.94 μg/m^3 (11 % of the total emissions) (Fig. 5), with the major contribution from OC (4.46 μg/m^3) and ions (cations = 3.21 μg/m^3, anions = 3.73 μg/m^3). The % FT of OC, SO_4^{2-}, NH_4^+ and NO_3^- were observed as 37.3 %, 25 %, 19 % and 16 %, while the SS % are 24.8 %, 19.77 %, 14.6 % and 58.6 % to the total PM, respectively (Fig. 5a). For pre-Diwali 2020, average SOC of 20.84 μg/m^3 was observed and the SA formation was also noted to be high during the same period. Presence of high OC during pre-Diwali 2020 might have aided in the formation of secondary organic aerosol (SOAs).

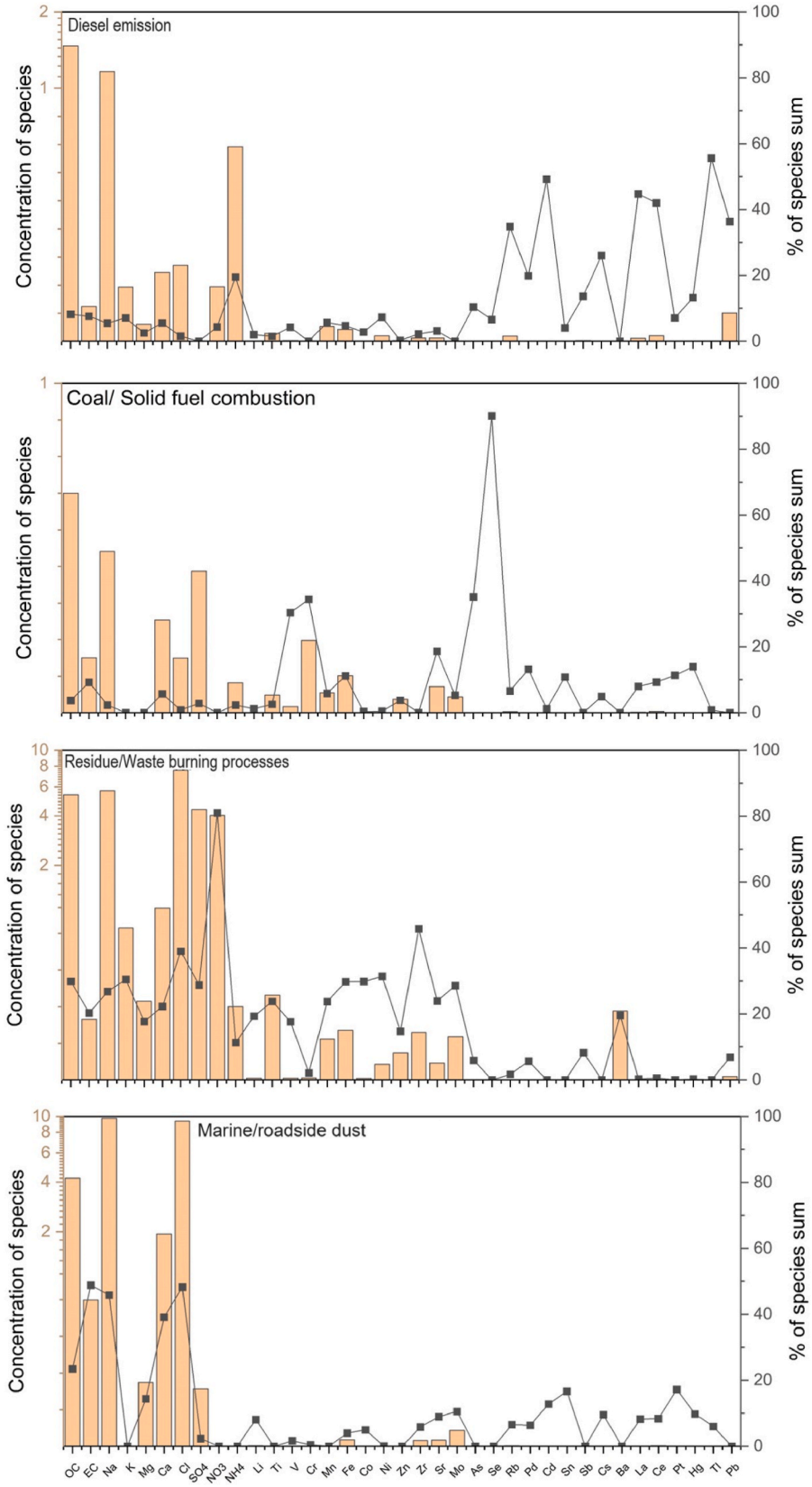

Fig. 5. (*continued*).

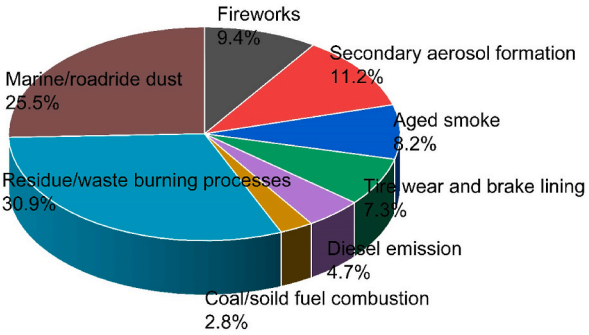

Fig. 6. Percentage contribution of different factors obtained from EPA-PMF model in the total PM_{10} concentration.

Secondary aerosol formation is a complex process involving the transformation of these pollutants into solid or liquid particles in the atmosphere. Here, the presence of NO_3^- and NH_4^+ might have assisted the formation of HNO_3 and $((NH_4)_2NO_3)$. These compounds are important constituents of SA [156].

4.8.1.3. Factor-3: industrial emissions with aged smoke. The contribution of Factor-3 to the overall emission was 8.71 μg/m^3 (8.2 %) (Fig. 5). Major contributors were the total metals (2.30 μg/m^3) and ions (cations = 2.63 μg/m^3, anions = 2.83 μg/m^3) to it. Chemical species contributing in terms of % FT were OC (10.44 %), SO_4^{2-} (32.43 %), K^+ (12.30 %), Mn (3.03 %), Ti (6.74 %), Fe (3.31 %), Zn (3.44 %), Zr (2.98 %), Mo (3.7 %), while in terms of SS%, these were K^+ (35.38 %), SO_4^{2-} (18.6 %), Li (31 %), Ti (27.2 %), Mn (25.24 %), Fe (28.53 %), Co (30.7 %), Ni (34.2 %), Zn (26.8 %), Zr (41.3 %), Mo (35.2 %) (Fig. 5a). Several studies have identified Zn, As, K^+, V as markers to emission from iron and steel industries [157]. Emissions of Zn, Mn and Cu are from non-ferrous sources [158,159], while V, Br are sourced from textile and S, Cu, Ni and V are from oil refinery [158]. Cr is contributed from electroplating and Cd from smelting industries.

A relationship between K^+ and SO_4^{2-} (Fig. S8) is utilized as a marker for the formation of aged smoke [160]. The present study found a positive correlation between K^+ and SO_4^{2-} ($R^2 = 0.78$; $P < 0.05$) (Figs. S7 and S8). High FRP (Fig. S3) and airmass transported to the sampling location suggests the persistent atmospheric BB and fossil fuels constituents, leading to the formation of aged smoke. Due to the presence of tracers from industries and strong K^+ vs SO_4^{2-} correlations, Factor-3 was identified as industrial emission with aged smoke. The relationship of K^+ and SO_4^{2-} could lead to the formation of K_2SO_4 and its long-range transport was responsible for the contribution of aged smoke [160,161].

4.8.1.4. Factor-4: vehicular emissions (brake linings and tire wear). The total concentration of Factor-4 to the overall contribution was 7.75 μg/m^3 (7.3 %) (Fig. 5). The concentration of cations (anions) and total metals were 3.51 μg/m^3 (1.88 μg/m^3) and 2.12 μg/m^3, along with OC of 0.24 μg/m^3. The % FT for Cl^-, Na^+, Mg^{2+}, Ti, Cr, Zn and OC were 24.29 %, 26.06 %, 11.5 %, 9.85 %, 5.20 %, 4.25 % and 3.04 %, hence, they were considered as tracers for this factor (Fig. 5a). Ni–Cr are associated with the emission from vehicular Ni–Cr based catalytic convertor [158]. Cr, Zn and Ti are emitted from brake, tire and engine wear [162]. Ca and Cl are used in lubricant oil in vehicles and diesel vehicles [163,164]. The presence of Mg^{2+} could be due to its presence in liquid fuel [165].

4.8.1.5. Factor-5: diesel emissions. The total contribution of Factor-5 to the total PM was 5 μg/m^3 (4.7 %). The contribution from cations, anions and total metals to the total PM were 50 % (2.5 μg/m^3), 10% (0.5 μg/m^3) and 29.5 % (1.47 μg/m^3) for this factor. The contribution of Na^+, NH_4^+ and OC were 5.5, 20 and 8.2% (Fig. 5b). The concentration of NH_4^+ dominate for this factor, followed by Pb. In the urban environment of Raipur, Chhattisgarh, NH_4^+, Pb and OC originated from three-wheeler vehicle (diesel) [166]. A study suggested reactive uptake of NH_3 in the formation of SOA [167]. Due to the presence of NH_4^+, Pb and OC, the factor can be considered as contribution from diesel emissions.

4.8.1.6. Factor-6: solid fuel/coal combustion. The contribution of this factor to the total concentration of PM was 2.95 μg/m^3 (2.8 %), and was lowest for both Diwali periods of 2019 and 2020. The % SS of Se and As were 90 % and 35.1 %, respectively along with V and Cr of 30.4 % and 34.5 %. The % FT were 22.6 % for OC, 14.58 % for SO_4^{2-} and 7.45 % for Cr to the total factor contribution (Fig. 5b). For this study, Se and As were considered as important tracers for coal combustion [168,169].

4.8.1.7. Factor-7: residue/waste burning processes. The contribution of this factor to the total concentration was 32.81 μg/m^3 (31 %), which was highest among all factors. The % SS of OC, EC, K^+, Ca^{2+}, Na^+ and Cl^- were 29.89 %, 20.28 %, 30.5 %, 22.25 %, 26.79 % and 39 %, respectively, while the % FT of OC, Cl, SO_4^{2-} and NO_3^- were 16.36 %, 23.1 %, 13.32 % and 12.3 % (Fig. 5b). For this study, NO_3^-, OC, K^+, Cl^- and Zr are considered as markers to BB and residue burning [112]. Cl^- is mainly observed in BB plumes. High NO_3^- (SS % of 81.04 %) and Ba (SS % of 19.55 %), on Diwali night and the following night were mainly emitted from fireworks. Presence of high NO_3^- supports the availability of NOx, which could be formed from OH° and O_3 [170]. Night of Diwali and its following night contribute to about 30 % of the total biomass burning emission. A combined effect of both fireworks and BB/residue burning was observed during

the sampling period for Hyderabad. A study over Delhi also observed effects of firework and transported crop residue burning emission [29,30]. Diwali night-time samples exhibited increased concentration of Factor-7 (residue and waste burning processes) for both 2019 and 2020 and corroborate the same for Factor-1, classified as fireworks. The increase in residue and waste burning processes could be due to burning of firecracker chemicals and its make-up/raw materials.

4.8.1.8. Factor-8: marine/roadside dust. The total contribution of this factor to the overall emission was 27.14 μg/m^3 (25.5 %) (Fig. 5). Contribution from major ions was 12.06 μg/m^3 (cations) and 9.73 μg/m^3 (anions), along with 0.24 μg/m^3 of TM and 4.22 μg/m^3 of OC. The % SS for Na^+, Cl^-, Ca^{2+}, OC and EC were 46 %, 48.3 %, 39 %, 23.5 % and 48 %, while the % FT of OC, Na^+, Cl^- and Ca^{2+} were 15.6 %, 35.6 %, 34.6 % and 7 %, respectively (Fig. 5b). Na^+, Cl^-, Ca^{2+}, OC and EC were considered as tracers for Factor-8. The presence of high concentrations of Na^+, Ca^{2+} and Cl^- is largely due to presence of salts [125]. The contributions of Na^+ and Cl^- to the total concentration of this factor were 9.74 μg/m^3 (35.9 %) and 9.38 μg/m^3 (34.6 %). The source for Ca^{2+} is soil dust [171]. Relatively higher moisture laden environment during Diwali period of 2019 affected the solubility and chemical reactivity of the particulates [172]. EC accumulates hygroscopic particles on its surface [173]. OC and aged EC during humid condition of 2019 may have aided in hygroscopic growth of particles, leading to the solubility of Ca^{2+}, Cl^- and Na^+ in the aerosols, compared to 2020, which was less humid.

According to EPA-PMF model, the source apportionment of aerosols suggested the highest contribution from BB/residue burning (35.2 μg/m^3), followed by marine/dust soil (27.1 μg/m^3). A combined effect of both fireworks and BB/residue burning was observed during the sampling period. The least contribution was observed for coal combustion during the sampling period, which was Se rich source, along with contribution from As, V, Cr. Total metallic contribution of 29 % was observed from fireworks. High crustal dust and vehicular emissions (brake linings, tire wear) were observed for pre-Diwali samples (Table S3), contributing about 44 % and 43 % to their respective sources.

5. Conclusion

This study investigated the chemical compositions of carbonaceous (OC and EC) and inorganic (REE, trace metals and major ions) constituents of aerosols, along with the isotopic composition of TC and EC fractions in PM_{10} samples collected during Diwali weeks of 2019 and 2020 in Hyderabad, Southern India. The results indicate increased concentration of the organic and inorganic constituents of PM_{10} during the night of Diwali for both the years. Contribution of secondary WSIIs (NH_4^+, NO_3^- and SO_4^{2-}), along with moisture availability during Diwali weeks suggested presence of deliquescent salts like NaCl, NH_4NO_3 and $(NH_4)_2SO_4$. K^+/Na^+ of 0.99 (0.74) and K^+_{nss}/OC of 1.37 (0.79) during the night of Diwali for 2019 (2020), respectively can be considered as an indicator for fireworks. Significant increase in metallic tracers (Ba, Pb, Sb, Sr and Fe) were observed during the nights of Diwali for both years. EPA-PMF model identified 8 different sources of aerosols, wherein BB/residue burning and fireworks contributed about 35.2 and 9.98 μg/m^3 during the Diwali weeks. Presence of K_2SO_4 suggested long-range transport of aged smoke. Isotopic composition of TC ($\delta^{13}C_{TC}$) did not show considerable influence of firecrackers, instead, it reflected the signature from emissions of diesel and C_3 plant burnings. Air-mass back trajectories along with the fire count (FRP) corroborated the long-range transport of BB/CRB emission to the sampling site. For most samples, $\delta^{13}C_{OC} > \delta^{13}C_{EC}$ indicated photochemical aging of aerosols during long-range transport. For pre-Diwali 2019 and post-Diwali 2020, $\delta^{13}C_{EC} > \delta^{13}C_{OC,}$ along with high OC/EC ratio and toluene suggested fresh SOA formation. Miller-Tans analyses suggested end-members for TC, OC to be diesel and C_3 plant burning, while for EC, these were C_3 plant burning, liquid fuel and coal combustion. Since studies in tropical region predominately utilise $\delta^{13}C$ of TC to apportion the sources, future research can utilise the $\delta^{13}C$ of EC to define the sources of carbonaceous aerosols. Additionally, investigations on the effect of fireworks on atmospheric boundary layer can provide useful insights into atmospheric stability.

Data availability statement

The data is available at Mendeley data repository with accession number: 10.17632/c6n4n6ch9d.1 (Reserved DOI).

CRediT authorship contribution statement

Pradeep Attri: Writing – review & editing, Writing – original draft, Visualization, Validation, Software, Methodology, Investigation, Formal analysis, Data curation, Conceptualization. **Devleena Mani:** Writing – review & editing, Supervision, Resources, Project administration, Investigation, Funding acquisition, Conceptualization. **M. Satyanarayanan:** Writing – review & editing, Formal analysis. **D.V. Reddy:** Writing – review & editing, Formal analysis, Data curation. **Devender Kumar:** Resources. **Siddhartha Sarkar:** Writing – review & editing, Formal analysis. **Sanjeev Kumar:** Resources. **Prashant Hegde:** Writing – review & editing, Resources.

Declaration of competing interest

The authors declare that they have no known competing financial interests or personal relationships that could have appeared to influence the work reported in this paper.

Acknowledgements

The authors thank the Directors of Council of Scientific and Industrial Research - National Geophysical Research Institute (CSIR-NGRI), Hyderabad and Physical Research Laboratory, Ahmedabad for providing the necessary laboratory facilities for carrying out the analysis during the research work. PA and DMT thank MHRD (F11/9/2019-U3(A) UoH-Institute of Eminence (IoE) for providing financial assistance to carry this work.

Appendix A. Supplementary data

Supplementary data to this article can be found online at https://doi.org/10.1016/j.heliyon.2024.e26746.

References

[1] U.C. Dumka, D.G. Kaskaoutis, D. Francis, J.P. Chaboureau, A. Rashki, S. Tiwari, S. Singh, E. Liakakou, N. Mihalopoulos, The role of the Intertropical discontinuity region and the heat low in dust emission and transport over the thar desert, India: a premonsoon case study, J. Geophys. Res. Atmos. (2019), https://doi.org/10.1029/2019JD030836.
[2] D.G. Kaskaoutis, K. Petrinoli, G. Grivas, P. Kalkavouras, M. Tsagkaraki, K. Tavernaraki, N. Mihalopoulos, Impact of Peri-Urban Forest Fires on Air Quality and Aerosol Optical and Chemical Properties: the Case of the August 2021 Wildfires in Athens, Greece, Sci. Total Environ. 907 (2024) 168028, https://doi.org/10.1016/j.scitotenv.2023.168028.
[3] G.L. Shi, G.R. Liu, Y.Z. Tian, X.Y. Zhou, X. Peng, Y.C. Feng, Chemical characteristic and toxicity assessment of particle associated PAHs for the short-term anthropogenic activity event: during the Chinese New Year's Festival in 2013, Sci. Total Environ. (2014), https://doi.org/10.1016/j.scitotenv.2014.02.107.
[4] V. Goel, N. Hazarika, M. Kumar, V. Singh, Source apportionment of black carbon over Delhi: a case study of extreme biomass burning events and Diwali festival, Urban Clim. (2021), https://doi.org/10.1016/j.uclim.2021.100926.
[5] C. Manchanda, M. Kumar, V. Singh, N. Hazarika, M. Faisal, V. Lalchandani, A. Shukla, J. Dave, N. Rastogi, S.N. Tripathi, Chemical speciation and source apportionment of ambient PM2.5 in New Delhi before, during, and after the Diwali fireworks, Atmos. Pollut. Res. 13 (6) (2022) 101428, https://doi.org/10.1016/j.apr.2022.101428.
[6] Ravindra, A.K. Mittal, R. Van Grieken, Health risk assessment of urban suspended particulate matter with special reference to polycyclic aromatic hydrocarbons: a review, Rev. Environ. Health (2001), https://doi.org/10.1515/REVEH.2001.16.3.169.
[7] Y. Wang, G. Zhuang, C. Xu, Z. An, The Air Pollution Caused by the Burning of Fireworks during the Lantern Festival in Beijing, Atmos. Environ. (2007), https://doi.org/10.1016/j.atmosenv.2006.07.043.
[8] M.S. Haque, R.B. Singh, Air pollution and human health in Kolkata, India: a case study, Climate (2017), https://doi.org/10.3390/cli5040077.
[9] S.C. Barman, R. Singh, M.P.S. Negi, S.K. Bhargava, Ambient air quality of lucknow city (India) during use of fireworks on diwali festival, Environ. Monit. Assess. 137 (1–3) (2008) 495–504, https://doi.org/10.1007/s10661-007-9784-1.
[10] B. Ambade, The air pollution during diwali festival by the burning of fireworks in Jamshedpur City, India, Urban Clim. (2018), https://doi.org/10.1016/j.uclim.2018.08.009.
[11] N. Kulshreshtha, S. Kumar, R.C. Vaishya, Assessment of trace metal concentration in the ambient air of the Prayagraj City during Diwali festival—a case study, Environ. Monit. Assess. (2021), https://doi.org/10.1007/s10661-021-08932-3.
[12] P.P. Khobragade, A.V. Ahirwar, Assessment of suspended particulate matter and heavy metal analysis during Diwali festival, J. Environ. Eng. Sci. (2022), https://doi.org/10.1680/jenes.21.00020.
[13] S. Sarkar, P.S. Khillare, D.S. Jyethi, A. Hasan, M. Parween, Chemical speciation of respirable suspended particulate matter during a major firework festival in India, J. Hazard Mater. (2010), https://doi.org/10.1016/j.jhazmat.2010.08.039.
[14] V.S. Yerramsetti, A.R. Sharma, N. Gauravarapu Navlur, V. Rapolu, N.S.K.C. Dhulipala, P.R. Sinha, The impact assessment of Diwali fireworks emissions on the air quality of a tropical urban site, Hyderabad, India, during three consecutive years, Environ. Monit. Assess. 185 (9) (2013) 7309–7325, https://doi.org/10.1007/s10661-013-3102-x.
[15] N. Rastogi, A. Singh, R. Satish, Characteristics of submicron particles coming from a big firecrackers burning event: implications to atmospheric pollution, Atmos. Pollut. Res. (2019), https://doi.org/10.1016/j.apr.2018.11.002.
[16] D.P. Singh, R. Gadi, T.K. Mandal, C.K. Dixit, K. Singh, T. Saud, N. Singh, P.K. Gupta, Study of temporal variation in ambient air quality during Diwali festival in India, Environ. Monit. Assess. 169 (1–4) (2010) 1–13, https://doi.org/10.1007/s10661-009-1145-9.
[17] A. Chatterjee, C. Sarkar, A. Adak, U. Mukherjee, S.K. Ghosh, S. Raha, Ambient air quality during Diwali festival over Kolkata - a mega-city in India, Aerosol Air Qual. Res. (2013), https://doi.org/10.4209/aaqr.2012.03.0062.
[18] A. Chatterjee, C. Sarkar, A. Adak, U. Mukherjee, S.K. Ghosh, S. Raha, Ambient air quality during diwali festival over Kolkata - a mega-city in India, Aerosol Air Qual. Res. 13 (3) (2013) 1133–1144, https://doi.org/10.4209/aaqr.2012.03.0062.
[19] Shivani, R. Gadi, M. Saxena, S.K. Sharma, T.K. Mandal, Short-term degradation of air quality during major firework events in Delhi, India, Meteorol. Atmos. Phys. (2019), https://doi.org/10.1007/s00703-018-0602-9.
[20] P. Rajput, A.K. Singh, K. Biswas, A.M. Qadri, T. Gupta, Source contribution of firecrackers burst vs. Long-range transport of biomass burning emissions over an urban background, Front. Sustain. Cities 2 (2021) 1–13, https://doi.org/10.3389/frsc.2020.622050.
[21] K. Li, J. Li, S. Tong, W. Wang, R.J. Huang, M. Ge, Characteristics of wintertime VOCs in suburban and urban Beijing: Concentrations, emission ratios, and festival effects, Atmos. Chem. Phys. (2019), https://doi.org/10.5194/acp-19-8021-2019.
[22] J.W. Fitzgerald, Marine aerosols: a review, Atmos. Environ. Part A, Gen. Top. (1991), https://doi.org/10.1016/0960-1686(91)90050-H.
[23] K.J. Godri, D.C. Green, G.W. Fuller, M. Dall'osto, D.C. Beddows, F.J. Kelly, R.M. Harrison, I.S. Mudway, Particulate oxidative burden associated with Firework activity, Environ. Sci. Technol. (2010), https://doi.org/10.1021/es1016284.
[24] A.K. Attri, U. Kumar, V.K. Jain, Formation of ozone by fireworks, Nature (2001), https://doi.org/10.1038/35082634.
[25] B.P. Singh, A.K. Srivastava, S. Tiwari, S. Singh, R.K. Singh, D.S. Bisht, D.M. Lal, A.K. Singh, R.K. Mall, M.K. Srivastava, Radiative impact of fireworks at a tropical Indian location: a case study, Adv. Meteorol. (2014), https://doi.org/10.1155/2014/197072.
[26] P.C.S. Devara, K. Vijayakumar, P.D. Safai, M.P. Raju, P.S.P. Rao, Celebration-induced air quality over a tropical urban station, Pune, India, Atmos. Pollut. Res. (2015), https://doi.org/10.5094/APR.2015.057.
[27] A. Chhabra, T. Turakhia, S. Sharma, S. Saha, R. Iyer, P. Chauhan, Environmental impacts of fireworks on aerosol characteristics and radiative properties over a mega city, India, City Environ. Int. (2020), https://doi.org/10.1016/j.cacint.2020.100049.
[28] H. Jethva, O. Torres, R.D. Field, A. Lyapustin, R. Gautam, V. Kayetha, Connecting crop productivity, residue fires, and air quality over northern India, Sci. Rep. (2019), https://doi.org/10.1038/s41598-019-52799-x.
[29] P. Saxena, A. Srivastava, S. Verma, Shweta, L. Singh, S. Sonwani, Analysis of atmospheric pollutants during fireworks festival 'diwali' at a residential site Delhi in India, 91–105, Energy, Environ., Sustain. (2020), https://doi.org/10.1007/978-981-15-0540-9_4.

[30] P. Saxena, A. Srivastava, S. Verma, Shweta, L. Singh, S. Sonwani, Analysis of atmospheric pollutants during fireworks festival 'diwali' at a residential site Delhi in India, Energy, Environ., Sustain. (2020), https://doi.org/10.1007/978-981-15-0540-9_4.

[31] D. Widory, Combustibles, fuels and their combustion products: a view through carbon isotopes, Combust. Theor. Model. (2006), https://doi.org/10.1080/13647830600720264.

[32] R. Agnihotri, T.K. Mandal, S.G. Karapurkar, M. Naja, R. Gadi, Y.N. Ahammmed, A. Kumar, T. Saud, M. Saxena, Stable carbon and nitrogen isotopic composition of bulk aerosols over India and Northern Indian Ocean, Atmos. Environ. (2011), https://doi.org/10.1016/j.atmosenv.2011.03.003.

[33] R. Agnihotri, S.G. Karapurkar, V.V.S.S. Sarma, K. Yadav, M.D. Kumar, C. Sharma, M.V.S.N. Prasad, Stable isotopic and chemical characteristics of bulk aerosols during winter and summer season at a station in Western Coast of India (Goa), Aerosol Air Qual. Res. (2015), https://doi.org/10.4209/aaqr.2014.07.0127.

[34] E.N. Kirillova, A. Andersson, R.J. Sheesley, M. Kruså, P.S. Praveen, K. Budhavant, P.D. Safai, P.S.P. Rao, Ö. Gustafsson, ^{13}C- and ^{14}C-based study of sources and atmospheric processing of water-soluble organic carbon (WSOC) in South Asian aerosols, J. Geophys. Res. Atmos. (2013), https://doi.org/10.1002/jgrd.50130.

[35] A. Andersson, J. Deng, K. Du, M. Zheng, C. Yan, M. Sköld, Ö. Gustafsson, Regionally-varying combustion sources of the january 2013 severe haze events over eastern China, Environ. Sci. Technol. (2015), https://doi.org/10.1021/es503855e.

[36] D. Widory, S. Roy, Y. Le Moullec, G. Goupil, A. Cocherie, C. Guerrot, The origin of atmospheric particles in Paris: A view through carbon and lead isotopes, Atmos. Environ. (2004), https://doi.org/10.1016/j.atmosenv.2003.11.001.

[37] H. Bai, X. Liu, X. Liu, C. Zhang, L. Mu, L. Peng, Carbon isotope seasonal characteristics of fine carbonaceous aerosol in Jinzhong City, Shanxi Province, China, Atmos. Environ. (2021), https://doi.org/10.1016/j.atmosenv.2020.118164.

[38] S. Irei, J. Rudolph, L. Huang, J. Auld, D. Hastie, Stable carbon isotope ratio of secondary particulate organic matter formed by photooxidation of toluene in indoor smog chamber, Atmos. Environ. (2011), https://doi.org/10.1016/j.atmosenv.2010.11.021.

[39] S.S. Babu, K.K. Moorthy, Anthropogenic impact on aerosol black carbon mass concentration at a tropical coastal station: a case study, Curr. Sci. 81 (2001) 1208–1214.

[40] U.C. Kulshrestha, T. Nageswara Rao, S. Azhaguvel, M.J. Kulshrestha, Emissions and accumulation of metals in the atmosphere due to crackers and sparkles during Diwali festival in India, Atmos. Environ. (2004), https://doi.org/10.1016/j.atmosenv.2004.05.044.

[41] S. Gummeneni, Y. Bin Yusup, M. Chavali, S.Z. Samadi, Source apportionment of particulate matter in the ambient air of Hyderabad city, India, Atmos. Res. (2011), https://doi.org/10.1016/j.atmosres.2011.05.002.

[42] V.K. Prasad, K.V.S. Badarinath, A. Eaturu, Biophysical and anthropogenic controls of forest fires in the Deccan Plateau, India, J. Environ. Manag. (2008), https://doi.org/10.1016/j.jenvman.2006.11.017.

[43] K.P. Vadrevu, K. Lasko, L. Giglio, C. Justice, Vegetation fires, absorbing aerosols and smoke plume characteristics in diverse biomass burning regions of Asia, Environ. Res. Lett. (2015), https://doi.org/10.1088/1748-9326/10/10/105003.

[44] A. Thomas, C. Sarangi, V.P. Kanawade, Recent increase in winter hazy days over Central India and the Arabian sea, Sci. Rep. (2019), https://doi.org/10.1038/s41598-019-53630-3.

[45] K.V.S. Badarinath, A.R. Sharma, S.K. Kharol, V.K. Prasad, Variations in CO, O3 and black carbon aerosol mass concentrations associated with planetary boundary layer (PBL) over tropical urban environment in India, J. Atmos. Chem. (2009), https://doi.org/10.1007/s10874-009-9137-2.

[46] D.G. Kaskaoutis, K.V.S. Badarinath, S.K. Kharol, A.R. Sharma, H.D. Kambezidis, Variations in the aerosol optical properties and types over the tropical urban site of Hyderabad, India, J. Geophys. Res. Atmos. (2009), https://doi.org/10.1029/2009JD012423.

[47] S.K. Kharol, K.V.S. Badarinath, A.R. Sharma, D.G. Kaskaoutis, H.D. Kambezidis, Multiyear analysis of Terra/Aqua MODIS aerosol optical depth and ground observations over tropical urban region of Hyderabad, India, Atmos. Environ. (2011), https://doi.org/10.1016/j.atmosenv.2010.12.047.

[48] P.R. Sinha, R.K. Manchanda, D.G. Kaskaoutis, Y.B. Kumar, S. Sreenivasan, Seasonal variation of surface and vertical profile of aerosol properties over a tropical urban station hyderabad, India, J. Geophys. Res. Atmos. (2013), https://doi.org/10.1029/2012JD018039.

[49] P. Attri, S. Sarkar, D. Mani, Classification and transformation of aerosols over selected Indian cities during reduced emissions under Covid-19 lockdown, J. Earth Syst. Sci. (2022), https://doi.org/10.1007/s12040-022-01916-y.

[50] Census of India 2011 Obtained from https://censusindia.gov.in/census.website/data/census-tables.

[51] H.S. Bhowmik, S. Naresh, D. Bhattu, N. Rastogi, A.S.H. Prévôt, S.N. Tripathi, Temporal and spatial variability of carbonaceous species (EC; OC; WSOC and SOA) in PM2.5 aerosol over five sites of Indo-Gangetic Plain, Atmos. Pollut. Res. (2021), https://doi.org/10.1016/j.apr.2020.09.019.

[52] H.S. Bhowmik, A. Shukla, V. Lalchandani, J. Dave, N. Rastogi, M. Kumar, V. Singh, S.N. Tripathi, Inter-comparison of online and offline methods for measuring ambient heavy and trace elements and water-soluble inorganic ions (NO3-, SO42-, NH4+, and Cl-) in PM2.5over a heavily polluted megacity, Delhi, Atmos. Meas. Tech. (2022), https://doi.org/10.5194/amt-15-2667-2022.

[53] D.V. Reddy, P. Nagabhushanam, B.S. Sukhija, A.G.S. Reddy, P.L. Smedley, Fluoride dynamics in the granitic aquifer of the Wailapally watershed, Nalgonda District, India, Chem. Geol. (2010), https://doi.org/10.1016/j.chemgeo.2009.10.003.

[54] X. Querol, J. Pey, M.C. Minguillón, N. Pérez, A. Alastuey, M. Viana, T. Moreno, R.M. Bernabé, S. Blanco, B. Cárdenas, E. Vega, G. Sosa, S. Escalona, H. Ruiz, B. Artíñano, PM speciation and sources in Mexico during the MILAGRO-2006 campaign, Atmos. Chem. Phys. (2008), https://doi.org/10.5194/acp-8-111-2008.

[55] M.C. Minguillón, X. Querol, U. Baltensperger, A.S.H. Prévôt, Fine and coarse PM composition and sources in rural and urban sites in Switzerland: local or regional pollution? Sci. Total Environ. (2012) https://doi.org/10.1016/j.scitotenv.2012.04.030.

[56] V. Balaram, M. Satyanarananan, D.V. Avdeev, N. Berdnikov, P. Roy, S.S. Sawant, K.S.V. Subramanyam, K.V. Anjaiah, C.T. Kamala, R. Mathur, B. Dasaram, Use or xenon as internal standard for the accurate determination of trace elements in water samples by ICP-MS, Atom. Spectros (2012), https://doi.org/10.46770/as.2012.02.001.

[57] M. Satyanarayanan, V. Balaram, S.S. Sawant, K.S.V. Subramanyam, G.V. Krishna, B. Dasaram, C. Manikyamba, Rapid determination of REEs, PGEs, and other trace elements in geological and environmental materials by high resolution inductively coupled plasma mass spectrometry, Atom. Spectros (2018), https://doi.org/10.46770/as.2018.01.001.

[58] P. Kumar, S. Yadav, Seasonal variations in water soluble inorganic ions, OC and EC in PM10 and PM>10 aerosols over Delhi: influence of sources and meteorological factors, Aerosol Air Qual. Res. (2016), https://doi.org/10.4209/aaqr.2015.07.0472.

[59] N.J. Spada, N.P. Hyslop, Comparison of elemental and organic carbon measurements between IMPROVE and CSN before and after method transitions, Atmos. Environ. (2018), https://doi.org/10.1016/j.atmosenv.2018.01.043.

[60] Ö. Gustafsson, F. Haghseta, C. Chan, J. Macfarlane, P.M. Gschwend, Quantification of the dilute sedimentary soot phase: implications for PAH speciation and bioavailability, Environ. Sci. Technol. (1997), https://doi.org/10.1021/es960317s.

[61] Ö. Gustafsson, T.D. Bucheli, Z. Kukulska, M. Andersson, C. Largeau, J.N. Rouzaud, C.M. Reddy, T.I. Eglinton, Evaluation of a protocol for the quantification of black carbon in sediments, Global Biogeochem. Cycles (2001), https://doi.org/10.1029/2000GB001380.

[62] Z. Zencak, M. Elmquist, Ö. Gustafsson, Quantification and radiocarbon source apportionment of black carbon in atmospheric aerosols using the CTO-375 method, Atmos. Environ. (2007), https://doi.org/10.1016/j.atmosenv.2007.06.006.

[63] P. Yao, R.J. Huang, H. Ni, N. Kairys, L. Yang, H.A.J. Meijer, U. Dusek, 13C signatures of aerosol organic and elemental carbon from major combustion sources in China compared to worldwide estimates, Sci. Total Environ. (2022), https://doi.org/10.1016/j.scitotenv.2021.151284.

[64] R.J. Sheesley, E. Kirillova, A. Andersson, M. Krusa, P.S. Praveen, K. Budhavant, P.D. Safai, P.S.P. Rao, O. Gustafsson, Year-round radiocarbon-based source apportionment of carbonaceous aerosols at two background sites in South Asia, J. Geophys. Res. Atmos. (2012), https://doi.org/10.1029/2011JD017161.

[65] S. Bikkina, A. Andersson, M.M. Sarin, R.J. Sheesley, E. Kirillova, R. Rengarajan, A.K. Sudheer, K. Ram, Ö. Gustafsson, Dual carbon isotope characterization of total organic carbon in wintertime carbonaceous aerosols from northern India, J. Geophys. Res. Atmos. (2016), https://doi.org/10.1002/2016JD024880.

[66] J.D. Blando, B.J. Turpin, Secondary organic aerosol formation in cloud and fog droplets: a literature evaluation of plausibility, Atmos. Environ. (2000), https://doi.org/10.1016/S1352-2310(99)00392-1.

[67] X.Y. Yu, R.A. Cary, N.S. Laulainen, Primary and secondary organic carbon downwind of Mexico City, Atmos. Chem. Phys. (2009), https://doi.org/10.5194/acp-9-6793-2009.

[68] Y. Miyazaki, Y. Kondo, N. Takegawa, Y. Komazaki, M. Fukuda, K. Kawamura, M. Mochida, K. Okuzawa, R.J. Weber, Time-resolved measurements of water-soluble organic carbon in Tokyo, J. Geophys. Res. Atmos. (2006), https://doi.org/10.1029/2006JD007125.

[69] Z.B. Yuan, J.Z. Yu, A.K.H. Lau, P.K.K. Louie, J.C.H. Fung, Application of positive matrix factorization in estimating aerosol secondary organic carbon in Hong Kong and its relationship with secondary sulfate, Atmos. Chem. Phys. (2006), https://doi.org/10.5194/acp-6-25-2006.

[70] H.J. Lim, B.J. Turpin, Origins of primary and secondary organic aerosol in Atlanta: Results of time-resolved measurements during the Atlanta Supersite Experiment, Environ. Sci. Technol. (2002), https://doi.org/10.1021/es0206487.

[71] C. Wu, J.Z. Yu, Determination of primary combustion source organic carbon-to-elemental carbon (OC/EC) ratio using ambient OC and EC measurements: secondary OC-EC correlation minimization method, Atmos. Chem. Phys. 16 (8) (2016) 5453–5465, https://doi.org/10.5194/acp-16-5453-2016.

[72] L.M. Castro, C.A. Pio, R.M. Harrison, D.J.T. Smith, Carbonaceous aerosol in urban and rural European atmospheres: estimation of secondary organic carbon concentrations, Atmos. Environ. (1999), https://doi.org/10.1016/S1352-2310(98)00331-8.

[73] D.G. Kaskaoutis, G. Grivas, C. Theodosi, M. Tsagkaraki, D. Paraskevopoulou, I. Stavroulas, E. Liakakou, A. Gkikas, N. Hatzianastassiou, C. Wu, E. Gerasopoulos, N. Mihalopoulos, Carbonaceous aerosols in contrasting atmospheric environments in Greek cities: evaluation of the EC-tracer methods for secondary organic carbon estimation, Atmosphere (2020), https://doi.org/10.3390/atmos11020161.

[74] D. Srivastava, K.R. Daellenbach, Y. Zhang, N. Bonnaire, B. Chazeau, E. Perraudin, V. Gros, F. Lucarelli, E. Villenave, A.S.H. Prévôt, I. El Haddad, O. Favez, A. Albinet, Comparison of five methodologies to apportion organic aerosol sources during a PM pollution event, Sci. Total Environ. (2021), https://doi.org/10.1016/j.scitotenv.2020.143168.

[75] J. Ringuet, A. Albinet, E. Leoz-Garziandia, H. Budzinski, E. Villenave, Diurnal/nocturnal concentrations and sources of particulate-bound PAHs, OPAHs and NPAHs at traffic and suburban sites in the region of Paris (France), Sci. Total Environ. (2012), https://doi.org/10.1016/j.scitotenv.2012.07.072.

[76] A. Albinet, S. Tomaz, F. Lestremau, A really quick easy cheap effective rugged and safe (QuEChERS) extraction procedure for the analysis of particle-bound PAHs in ambient air and emission samples, Sci. Total Environ. (2013), https://doi.org/10.1016/j.scitotenv.2013.01.068.

[77] A. Albinet, F. Nalin, S. Tomaz, J. Beaumont, F. Lestremau, A simple QuEChERS-like extraction approach for molecular chemical characterization of organic aerosols: application to nitrated and oxygenated PAH derivatives (NPAH and OPAH) quantified by GC-NICIMS, Anal. Bioanal. Chem. (2014), https://doi.org/10.1007/s00216-014-7760-5.

[78] J. Yu, C. Yan, Y. Liu, X. Li, T. Zhou, M. Zheng, Potassium: a tracer for biomass burning in Beijing? Aerosol Air Qual. Res. (2018) https://doi.org/10.4209/aaqr.2017.11.0536.

[79] Y. Cheng, G. Engling, K.B. He, F.K. Duan, Y.L. Ma, Z.Y. Du, J.M. Liu, M. Zheng, R.J. Weber, Biomass burning contribution to Beijing aerosol, Atmos. Chem. Phys. (2013), https://doi.org/10.5194/acp-13-7765-2013.

[80] Y.Z. Tian, J. Wang, X. Peng, G.L. Shi, Y.C. Feng, Estimation of the direct and indirect impacts of fireworks on the physicochemical characteristics of atmospheric PM10 and PM2.5, Atmos. Chem. Phys. (2014), https://doi.org/10.5194/acp-14-9469-2014.

[81] J.V. Puthussery, J. Dave, A. Shukla, S. Gaddamidi, A. Singh, P. Vats, S. Salana, D. Ganguly, N. Rastogi, S.N. Tripathi, V. Verma, Effect of biomass burning, diwali fireworks, and polluted fog events on the oxidative potential of fine ambient particulate matter in Delhi, India, Environ. Sci. Technol. (2022), https://doi.org/10.1021/acs.est.2c02730.

[82] C.D. Keeling, The concentration and isotopic abundances of atmospheric carbon dioxide in rural areas, Geochem. Cosmochim. Acta (1958), https://doi.org/10.1016/0016-7037(58)90033-4.

[83] J.B. Miller, P.P. Tans, Calculating isotopic fractionation from atmospheric measurements at various scales, Tellus Ser. B Chem. Phys. Meteorol. (2003), https://doi.org/10.1034/j.1600-0889.2003.00020.x.

[84] M. Devaprasad, N. Rastogi, R. Satish, A. Patel, A. Singh, A. Dabhi, A. Shivam, R. Bhushan, R. Meena, Characterization of paddy-residue burning derived carbonaceous aerosols using dual carbon isotopes, Sci. Total Environ. (2023), https://doi.org/10.1016/j.scitotenv.2022.161044.

[85] F. Amato, A. Alastuey, A. Karanasiou, F. Lucarelli, S. Nava, G. Calzolai, M. Severi, S. Becagli, V.L. Gianelle, C. Colombi, C. Alves, D. Custódio, T. Nunes, M. Cerqueira, C. Pio, K. Eleftheriadis, E. Diapouli, C. Reche, M.C. Minguillón, X. Querol, AIRUSE-LIFE+: a harmonized PM speciation and source apportionment in five southern European cities, Atmos. Chem. Phys. (2016), https://doi.org/10.5194/acp-16-3289-2016.

[86] U.S. EPA, EPA Positive Matrix Factorization (PM F) 5.0, User Guide, 2014.

[87] P.D. Safai, M.P. Raju, P.S.P. Rao, G. Pandithurai, Characterization of carbonaceous aerosols over the urban tropical location and a new approach to evaluate their climatic importance, Atmos. Environ. (2014), https://doi.org/10.1016/j.atmosenv.2014.04.055.

[88] M. Manousakas, H. Papaefthymiou, E. Diapouli, A. Migliori, A.G. Karydas, I. Bogdanovic-Radovic, K. Eleftheriadis, Assessment of PM2.5 sources and their corresponding level of uncertainty in a coastal urban area using EPA PMF 5.0 enhanced diagnostics, Sci. Total Environ. (2017), https://doi.org/10.1016/j.scitotenv.2016.09.047.

[89] S. Pervez, R.K. Chakrabarty, S. Dewangan, J.G. Watson, J.C. Chow, J.L. Matawle, Chemical speciation of aerosols and air quality degradation during the festival of lights (Diwali), Atmos. Pollut. Res. (2016), https://doi.org/10.1016/j.apr.2015.09.002.

[90] V.M. Kerminen, R. Hillamo, K. Teinilä, T. Pakkanen, I. Allegrini, R. Sparapani, Ion balances of size-resolved tropospheric aerosol samples: implications for the acidity and atmospheric processing of aerosols, Atmos. Environ. (2001), https://doi.org/10.1016/S1352-2310(01)00345-4.

[91] P. Saxena, A. Kumar, S.K. Mahanta, B. Sreekanth, D.K. Patel, A. Kumari, A.H. Khan, G.C. Kisku, Chemical characterization of PM10 and PM2.5 combusted firecracker particles during Diwali of Lucknow City, India: air-quality deterioration and health implications, Environ. Sci. Pollut. Control Ser. (2022), https://doi.org/10.1007/s11356-022-21906-3.

[92] J. Seinfeld, S. Pandis, Properties of the atmospheric aerosol, Atmos. Chem. Phys.: From Air Pollution to Climate Change (2006).

[93] X. Huang, R. Qiu, C.K. Chan, P. Ravi Kant, Evidence of high PM2.5 strong acidity in ammonia-rich atmosphere of Guangzhou, China: transition in pathways of ambient ammonia to form aerosol ammonium at [NH4+]/[SO42-]=1.5, Atmos. Res. (2011), https://doi.org/10.1016/j.atmosres.2010.11.021.

[94] S. Aryasree, P.R. Nair, P. Hegde, Radiative characteristics of near-surface aerosols at a tropical site: an estimation based on concurrent measurements of their physico-chemical characteristics, J. Earth Syst. Sci. (2020), https://doi.org/10.1007/s12040-020-01444-7.

[95] A. Kulshrestha, D.S. Bisht, J. Masih, D. Massey, S. Tiwari, A. Taneja, Chemical characterization of water-soluble aerosols in different residential environments of semi aridregion of India, J. Atmos. Chem. (2009), https://doi.org/10.1007/s10874-010-9143-4.

[96] R. Vecchi, V. Bernardoni, D. Cricchio, A. D'Alessandro, P. Fermo, F. Lucarelli, S. Nava, A. Piazzalunga, G. Valli, The impact of fireworks on airborne particles, Atmos. Environ. (2008), https://doi.org/10.1016/j.atmosenv.2007.10.047.

[97] H. ten Brink, R. Otjes, E. Weijers, Extreme levels and chemistry of PM from the consumer fireworks in The Netherlands, Atmos. Environ. (2019), https://doi.org/10.1016/j.atmosenv.2019.04.046.

[98] P.S. Rao, D.G. Gajghate, A.G. Gavane, P. Suryawanshi, C. Chauhan, S. Mishra, N. Gupta, C.V.C. Rao, S.R. Wate, Air quality status during diwali festival of India: a case study, Bull. Environ. Contam. Toxicol. (2012), https://doi.org/10.1007/s00128-012-0669-9.

[99] P.D. Safai, S. Kewat, G. Pandithurai, P.S. Praveen, K. Ali, S. Tiwari, P.S.P. Rao, K.B. Budhawant, S.K. Saha, P.C.S. Devara, Aerosol characteristics during winter fog at Agra, North India, J. Atmos. Chem. (2008), https://doi.org/10.1007/s10874-009-9127-4.

[100] A.R. Aswini, P. Hegde, P.R. Nair, Carbonaceous and inorganic aerosols over a sub-urban site in peninsular India: temporal variability and source characteristics, Atmos. Res. (2018), https://doi.org/10.1016/j.atmosres.2017.09.005.

[101] P. Bhuyan, P. Deka, A. Prakash, S. Balachandran, R.R. Hoque, Chemical characterization and source apportionment of aerosol over mid Brahmaputra Valley, India, Environ. Pollut. (2018), https://doi.org/10.1016/j.envpol.2017.12.009.

[102] H.W. Xiao, H.Y. Xiao, L. Luo, C.Y. Shen, A.M. Long, L. Chen, D.N. Li, Atmospheric aerosol compositions over the South China Sea: temporal variability and source apportionment, Atmos. Chem. Phys. 17 (4) (2017) 3199–3214, https://doi.org/10.5194/acp-17-3199-2017.

[103] L. Fourtziou, E. Liakakou, I. Stavroulas, C. Theodosi, P. Zarmpas, B. Psiloglou, J. Sciare, T. Maggos, K. Bairachtari, A. Bougiatioti, E. Gerasopoulos, R. Sarda-Estève, N. Bonnaire, N. Mihalopoulos, Multi-tracer approach to characterize domestic wood burning in Athens (Greece) during wintertime, Atmos. Environ. (2017), https://doi.org/10.1016/j.atmosenv.2016.10.011.
[104] E. Jung, B.A. Albrecht, H.H. Jonsson, Y.C. Chen, J.H. Seinfeld, A. Sorooshian, A.R. Metcalf, S. Song, M. Fang, L.M. Russell, Precipitation effects of giant cloud condensation nuclei artificially introduced into stratocumulus clouds, Atmos. Chem. Phys. (2015), https://doi.org/10.5194/acp-15-5645-2015.
[105] H. Dadashazar, L. Ma, A. Sorooshian, Sources of pollution and interrelationships between aerosol and precipitation chemistry at a central California site, Sci. Total Environ. (2019), https://doi.org/10.1016/j.scitotenv.2018.10.086.
[106] D.G. Kaskaoutis, G. Grivas, K. Oikonomou, P. Tavernaraki, K. Papoutsidaki, M. Tsagkaraki, I. Stavroulas, P. Zarmpas, D. Paraskevopoulou, A. Bougiatioti, E. Liakakou, M. Gavrouzou, U.C. Dumka, N. Hatzianastassiou, J. Sciare, E. Gerasopoulos, N. Mihalopoulos, Impacts of severe residential wood burning on atmospheric processing, water-soluble organic aerosol and light absorption, in an Inland City of Southeastern Europe, Atmos. Environ. (2022), https://doi.org/10.1016/j.atmosenv.2022.119139.
[107] A.F. Corral, H. Dadashazar, C. Stahl, E. Edwards, Lou, P. Zuidema, A. Sorooshian, Source apportionment of aerosol at a coastal site and relationships with precipitation chemistry: a case study over the southeast United States, Atmosphere (2020), https://doi.org/10.3390/atmos11111212.
[108] K. Adachi, P.R. Buseck, Changes in shape and composition of sea-salt particles upon aging in an urban atmosphere, Atmos. Environ. (2015), https://doi.org/10.1016/j.atmosenv.2014.10.036.
[109] Y. Qin, K. Oduyemi, L.Y. Chan, Comparative testing of PMF and CFA models, Chemometr. Intell. Lab. Syst. (2002), https://doi.org/10.1016/S0169-7439(01)00175-7.
[110] N. Pérez, J. Pey, C. Reche, J. Cortés, A. Alastuey, X. Querol, Impact of harbour emissions on ambient PM10 and PM2.5 in Barcelona (Spain): evidences of secondary aerosol formation within the urban area, Sci. Total Environ. (2016), https://doi.org/10.1016/j.scitotenv.2016.07.025.
[111] G. Kotnala, M. Kumar, A.K. Sharma, S.K. Dhaka, R. Gadi, barman, C. Ghosh, M. Saxena, S.K. Sharma, A.R. Saha, A. Nautiyal, A. Sharma, C. Sharma, R. K. Kotnala, T.K. Mandal, Variations in chemical composition of aerosol during Diwali over mega city Delhi, India, Urban Clim. (2021), https://doi.org/10.1016/j.uclim.2021.100991.
[112] A. Gaudichet, F. Echalar, B. Chatenet, J.P. Quisefit, G. Malingre, H. Cachier, P. Buat-Menard, P. Artaxo, W. Maenhaut, Trace elements in tropical African savanna biomass burning aerosols, J. Atmos. Chem. (1995), https://doi.org/10.1007/BF00708179.
[113] J. Noda, R. Bergström, X. Kong, T.L. Gustafsson, B. Kovacevik, M. Svane, J.B.C. Pettersson, Aerosol from biomass combustion in northern europe: influence of meteorological conditions and air mass history, Atmosphere (2019), https://doi.org/10.3390/ATMOS10120789.
[114] S. Tiwari, A.K. Srivastava, D.S. Bisht, T. Bano, S. Singh, S. Behura, M.K. Srivastava, D.M. Chate, B. Padmanabhamurty, Black carbon and chemical characteristics of PM10 and PM 2.5 at an urban site of North India, J. Atmos. Chem. (2009), https://doi.org/10.1007/s10874-010-9148-z.
[115] B. Ervens, B.J. Turpin, R.J. Weber, Secondary organic aerosol formation in cloud droplets and aqueous particles (aqSOA): a review of laboratory, field and model studies, Atmos. Chem. Phys. (2011), https://doi.org/10.5194/acp-11-11069-2011.
[116] R. Chesselet, J. Morelli, P. Buat-Menard, Variations in ionic ratios between reference sea water and marine aerosols, J. Geophys. Res. (1972), https://doi.org/10.1029/jc077i027p05116.
[117] Y. Mamane, Estimate of municipal refuse incinerator contribution to philadelphia aerosol-I. Source analysis, Atmos. Environ. 1967 (1988), https://doi.org/10.1016/0004-6981(88)90473-8.
[118] A. Ooki, M. Uematsu, K. Miura, S. Nakae, Sources of sodium in atmospheric fine particles, Atmos. Environ. (2002), https://doi.org/10.1016/S1352-2310(02)00341-2.
[119] A. Chakraborty, T. Gupta, A. Mandaria, S. Tripathi, Trace elements in ambient aerosols and size-resolved fog droplets: trends, enrichment, and risk assessment, Heliyon (2023) 1, https://doi.org/10.1016/j.heliyon.2023.e16400.
[120] M.O. Andreae, Soot carbon and excess fine potassium: long-range transport of combustion-derived aerosols, Science (1983), https://doi.org/10.1126/science.220.4602.1148.
[121] F. Duan, X. Liu, T. Yu, H. Cachier, Identification and estimate of biomass burning contribution to the urban aerosol organic carbon concentrations in Beijing, Atmos. Environ. (2004), https://doi.org/10.1016/j.atmosenv.2003.11.037.
[122] W. Sun, D. Wang, L. Yao, H. Fu, Q. Fu, H. Wang, Q. Li, L. Wang, X. Yang, A. Xian, G. Wang, H. Xiao, J. Chen, Chemistry-triggered events of PM2.5 explosive growth during late autumn and winter in Shanghai, China, Environ. Pollut. (2019), https://doi.org/10.1016/j.envpol.2019.07.032.
[123] M.O. Andreae, Emission of trace gases and aerosols from biomass burning - an updated assessment, Atmos. Chem. Phys. (2019), https://doi.org/10.5194/acp-19-8523-2019.
[124] F. Echalar, A. Gaudichet, H. Cachier, P. Artaxo, Aerosol emissions by tropical forest and savanna biomass burning: characteristic trace elements and fluxes, Geophys. Res. Lett. (1995), https://doi.org/10.1029/95GL03170.
[125] W.M.G. Lee, W.M. Huang, Y.Y. Chen, Effect of relative humidity on mixed aerosols in atmosphere, J. Environ. Sci. Health - A Toxic/Hazard. Subst. Environ. Eng. (2001), https://doi.org/10.1081/ESE-100103482.
[126] K. Ram, M.M. Sarin, S.N. Tripathi, A 1 year record of carbonaceous aerosols from an urban site in the Indo-Gangetic Plain: characterization, sources, and temporal variability, J. Geophys. Res. Atmos. (2010), https://doi.org/10.1029/2010JD014188.
[127] C.C. Lin, A review of the impact of fireworks on particulate matter in ambient air, J. Air Waste Manag. Assoc. (2016), https://doi.org/10.1080/10962247.2016.1219280.
[128] C. Hickey, C. Gordon, K. Galdanes, M. Blaustein, L. Horton, S. Chillrud, J. Ross, L. Yinon, L.C. Chen, T. Gordon, Toxicity of particles emitted by fireworks, Part. Fibre Toxicol. (2020), https://doi.org/10.1186/s12989-020-00360-4.
[129] C. Mocella, J.A. Conkling, Chemistry of Pyrotechnics: Basic Principles and Theory, CRC Press, 2019, https://doi.org/10.1201/9780429262135, 2019.
[130] P. Kulkarni, S. Chellam, M.P. Fraser, Tracking Petroleum refinery emission events using lanthanum and lanthanides as elemental markers for PM2.5, Environ. Sci. Technol. (2007), https://doi.org/10.1021/es062888i.
[131] R.L. Rudnick, S. Gao, Composition of the continental crust, in: K.K. Turekian (Ed.), Treatise on Geochemistry. Holland, 542 H.D., 3, Elsevier, Amsterdam, 2004, pp. 1–64, https://doi.org/10.1016/B0-08-043751-6/03016-4.
[132] G. Simonetti, E. Conte, C. Perrino, S. Canepari, Oxidative potential of size-segregated PM in an urban and an industrial area of Italy, Atmos. Environ. (2018), https://doi.org/10.1016/j.atmosenv.2018.05.051.
[133] G. Simonetti, D. Frasca, M. Marcoccia, C. Farao, S. Canepari, Multi-elemental analysis of particulate matter samples collected by a particle-into-liquid sampler, Atmos. Pollut. Res. (2018), https://doi.org/10.1016/j.apr.2018.01.006.
[134] P. Saxena, S. Sonwani, S.K. Sharma, P. Kumar, N. Chandra, Carbonaceous aerosol variations in foggy days: a critical analysis during the fireworks festival, Fresenius Environ. Bull. 29 (8) (2020) 6639–6656.
[135] P. Hegde, K. Kawamura, I.A. Girach, P.R. Nair, Characterisation of water-soluble organic aerosols at a site on the southwest coast of India, J. Atmos. Chem. (2016), https://doi.org/10.1007/s10874-015-9322-4.
[136] C.M. Pavuluri, K. Kawamura, S.G. Aggarwal, T. Swaminathan, Characteristics, seasonality and sources of carbonaceous and ionic components in the tropical aerosols from Indian region, Atmos. Chem. Phys. (2011), https://doi.org/10.5194/acp-11-8215-2011.
[137] S.G. Aggarwal, K. Kawamura, Molecular distributions and stable carbon isotopic compositions of dicarboxylic acids and related compounds in aerosols from Sapporo, Japan: implications for photochemical aging during long-range atmospheric transport, J. Geophys. Res. Atmos. (2008), https://doi.org/10.1029/2007JD009365.
[138] P. Kumar, S. Kumar, S. Yadav, Seasonal variations in size distribution, water-soluble ions, and carbon content of size-segregated aerosols over New Delhi, Environ. Sci. Pollut. Control Ser. (2018), https://doi.org/10.1007/s11356-017-0954-6.
[139] A.K. Singh, A. Srivastava, Seasonal variation of carbonaceous species in PM1 measured over residential area of Delhi, India, SN Appl. Sci. (2020), https://doi.org/10.1007/s42452-020-03854-0.

[140] P. hui Li, Y. Wang, T. Li, L. Sun, X. Yi, L. qiong Guo, R. hong Su, Characterization of carbonaceous aerosols at Mount Lu in South China: implication for secondary organic carbon formation and long-range transport, Environ. Sci. Pollut. Control Ser. (2015), https://doi.org/10.1007/s11356-015-4654-9.
[141] S. Hama, I. Ouchen, K.P. Wyche, R.L. Cordell, P.S. Monks, Carbonaceous aerosols in five European cities: insights into primary emissions and secondary particle formation, Atmos. Res. (2022), https://doi.org/10.1016/j.atmosres.2022.106180.
[142] P. Winiger, A. Andersson, K.E. Yttri, P. Tunved, Ö. Gustafsson, Isotope-based source apportionment of EC aerosol particles during winter high-pollution events at the Zeppelin observatory, svalbard, Environ. Sci. Technol. (2015), https://doi.org/10.1021/acs.est.5b02644.
[143] M. Hallquist, J.C. Wenger, U. Baltensperger, Y. Rudich, D. Simpson, M. Claeys, J. Dommen, N.M. Donahue, C. George, A.H. Goldstein, J.F. Hamilton, H. Herrmann, T. Hoffmann, Y. Iinuma, M. Jang, M.E. Jenkin, J.L. Jimenez, A. Kiendler-Scharr, W. Maenhaut, J. Wildt, The formation, properties and impact of secondary organic aerosol: current and emerging issues, Atmos. Chem. Phys. (2009), https://doi.org/10.5194/acp-9-5155-2009.
[144] S. Dasari, A. Andersson, A. Stohl, N. Evangeliou, H. Holmstrand, K. Budhavant, A. Salam, Ö. Gustafsson, Source quantification of South Asian black carbon aerosols with isotopes and modeling, Environ. Sci. Technol. (2020), https://doi.org/10.1021/acs.est.0c02193.
[145] H. Ni, R.J. Huang, J. Cao, W. Liu, T. Zhang, M. Wang, H.A.J. Meijer, U. Dusek, Source apportionment of carbonaceous aerosols in Xi'an, China: insights from a full year of measurements of radiocarbon and the stable isotope ^{13}C, Atmos. Chem. Phys. (2018), https://doi.org/10.5194/acp-18-16363-2018.
[146] H. Kawashima, Y. Haneishi, Effects of combustion emissions from the Eurasian continent in winter on seasonal δ13C of elemental carbon in aerosols in Japan, Atmos. Environ. (2012), https://doi.org/10.1016/j.atmosenv.2011.05.015.
[147] R. Sawlani, R. Agnihotri, C. Sharma, P.K. Patra, A.P. Dimri, K. Ram, R.L. Verma, The severe Delhi SMOG of 2016: a case of delayed crop residue burning, coincident firecracker emissions, and atypical meteorology, Atmos. Pollut. Res. 10 (3) (2019) 868–879, https://doi.org/10.1016/j.apr.2018.12.015.
[148] J. ji Cao, J.C. Chow, J. Tao, S. cheng Lee, J.G. Watson, K. Ho, Wang fai, G. hui, C. shu Zhu, Y. ming Han, Stable carbon isotopes in aerosols from Chinese cities: influence of fossil fuels, Atmos. Environ. (2011), https://doi.org/10.1016/j.atmosenv.2010.10.056.
[149] A.K. Sudheer, M.Y. Aslam, M. Upadhyay, R. Rengarajan, R. Bhushan, J.S. Rathore, S.K. Singh, S. Kumar, Carbonaceous aerosol over semi-arid region of western India: heterogeneity in sources and characteristics, Atmos. Res. (2016), https://doi.org/10.1016/j.atmosres.2016.03.026.
[150] C.C.W. Lee, J.H. Savarino, H. Cachier, M.H. Thiemens, Sulfur (32S,33S, 34S,36S) and oxygen (16O, 17O, 18O) isotopic ratios of primary sulfate produced from combustion processes, Tellus Ser. B Chem. Phys. Meteorol. (2002), https://doi.org/10.1034/j.1600-0889.2002.01384.x.
[151] T.C. Bond, S.J. Doherty, D.W. Fahey, P.M. Forster, T. Berntsen, B.J. Deangelo, M.G. Flanner, S. Ghan, B. Kärcher, D. Koch, S. Kinne, Y. Kondo, P.K. Quinn, M. C. Sarofim, M.G. Schultz, M. Schulz, C. Venkataraman, H. Zhang, S. Zhang, C.S. Zender, Bounding the role of black carbon in the climate system: a scientific assessment, J. Geophys. Res. Atmos. (2013), https://doi.org/10.1002/jgrd.50171.
[152] C. Bosch, A. Andersson, E.N. Kirillova, K. Budhavant, S. Tiwari, P.S. Praveen, L.M. Russell, N.D. Beres, V. Ramanathan, Ö. Gustafsson, Source-diagnostic dual-isotope composition and optical properties of water-soluble organic carbon and elemental carbon in the South Asian outflow intercepted over the Indian Ocean, J. Geophys. Res. (2014), https://doi.org/10.1002/2014JD022127.
[153] D.D. Dutcher, K.D. Perry, T.A. Cahill, S.A. Copeland, Effects of indoor pyrotechnic displays on the air quality in the houston astrodome, J. Air Waste Manag. Assoc. (1999), https://doi.org/10.1080/10473289.1999.10463790.
[154] T.M. Do, C.F. Wang, Y.K. Hsieh, H.F. Hsieh, Metals present in ambient air before and after a firework festival in Yanshui, Tainan, Taiwan, Aerosol Air Qual. Res. 12 (5) (2012) 981–993, https://doi.org/10.4209/aaqr.2012.03.0069.
[155] P.P. Khobragade, A.V. Ahirwar, Assessment of suspended particulate matter and heavy metal analysis during Diwali festival at Raipur, Chhattisgarh, India, J. Environ. Eng. Sci. (2022), https://doi.org/10.1680/jenes.21.00020.
[156] J. Gao, Y. Li, J. Li, G. Shi, Z. Liu, B. Han, X. Tian, Y. Wang, Y. Feng, A.G. Russell, Impact of formation pathways on secondary inorganic aerosol during haze pollution in Beijing: quantitative evidence from high-resolution observation and modeling, Geophys. Res. Lett. (2021), https://doi.org/10.1029/2021GL095623.
[157] J. Duan, J. Tan, Atmospheric heavy metals and Arsenic in China: situation, sources and control policies, Atmos. Environ. (2013), https://doi.org/10.1016/j.atmosenv.2013.03.031.
[158] B.S. Negi, S. Sadasivan, U.C. Mishra, Aerosol composition and sources in urban areas in India, Atmos. Environ. (1967), https://doi.org/10.1016/0004-6981(67)90072-8.
[159] S. Jain, S.K. Sharma, N. Choudhary, R. Masiwal, M. Saxena, A. Sharma, T.K. Mandal, A. Gupta, N.C. Gupta, C. Sharma, Chemical characteristics and source apportionment of PM2.5 using PCA/APCS, UNMIX, and PMF at an urban site of Delhi, India, Environ. Sci. Pollut. Control Ser. (2017), https://doi.org/10.1007/s11356-017-8925-5.
[160] J. Li, M. Pósfai, P.V. Hobbs, P.R. Buseck, Individual aerosol particles from biomass burning in southern Africa: 2. Compositions and aging of inorganic particles, J. Geophys. Res. Atmos. (2003), https://doi.org/10.1029/2002jd002310.
[161] Y. Zhou, T. Wang, X. Gao, L. Xue, X. Wang, Z. Wang, J. Gao, Q. Zhang, W. Wang, Continuous observations of water-soluble ions in PM2.5 at Mount Tai (1534 ma.s.l.) in central-eastern China, J. Atmos. Chem. (2009), https://doi.org/10.1007/s10874-010-9172-z.
[162] A. Thorpe, R.M. Harrison, Sources and properties of non-exhaust particulate matter from road traffic: a review, Sci. Total Environ. (2008), https://doi.org/10.1016/j.scitotenv.2008.06.007.
[163] M.T. Spencer, L.G. Shields, D.A. Sodeman, S.M. Toner, K.A. Prather, Comparison of oil and fuel particle chemical signatures with particle emissions from heavy and light duty vehicles, Atmos. Environ. (2006), https://doi.org/10.1016/j.atmosenv.2006.04.011.
[164] Jaiprakash, G. Habib, Chemical and optical properties of PM2.5 from on-road operation of light duty vehicles in Delhi city, Sci. Total Environ. (2017), https://doi.org/10.1016/j.scitotenv.2017.02.070.
[165] X. Querol, M. Viana, A. Alastuey, F. Amato, T. Moreno, S. Castillo, J. Pey, J. de la Rosa, A. Sánchez de la Campa, B. Artíñano, P. Salvador, S. García Dos Santos, R. Fernández-Patier, S. Moreno-Grau, L. Negral, M.C. Minguillón, E. Monfort, J.I. Gil, A. Inza, J. Zabalza, Source origin of trace elements in PM from regional background, urban and industrial sites of Spain, Atmos. Environ. (2007), https://doi.org/10.1016/j.atmosenv.2007.05.022.
[166] S. Pervez, S. Bano, J.G. Watson, J.C. Chow, J.L. Matawle, A. Shrivastava, Y.F. Pervez, Source profiles for PM10-2.5 resuspended dust and vehicle exhaust emissions in central India, Aerosol Air Qual. Res. 18 (7) (2018) 1660–1672, https://doi.org/10.4209/aaqr.2017.08.0259.
[167] Y. Liu, J. Liggio, R. Staebler, Reactive uptake of ammonia to secondary organic aerosols: kinetics of organonitrogen formation, Atmos. Chem. Phys. (2015), https://doi.org/10.5194/acp-15-13569-2015.
[168] P.D. Hien, N.T. Binh, Y. Truong, N.T. Ngo, L.N. Sieu, Comparative receptor modelling study of TSP, PM2 and PM2-10 in Ho chi minh city, Atmos. Environ. (2001), https://doi.org/10.1016/S1352-2310(00)00574-4.
[169] S. Lee, W. Liu, Y. Wang, A.G. Russell, E.S. Edgerton, Source apportionment of PM2.5: comparing PMF and CMB results for four ambient monitoring sites in the southeastern United States, Atmos. Environ. (2008), https://doi.org/10.1016/j.atmosenv.2008.01.025.
[170] K. Gupta, A. Saha, B. Sen Gupta, Spatio-temporal distribution of pollutant trace gases (CO, CH4, O3 and NO2) in India: an observational study, Geol., Ecol., Landscapes (2022), https://doi.org/10.1080/24749508.2022.2132706.
[171] U.C. Kulshrestha, M.J. Kulshrestha, R. Sekar, G.S.R. Sastry, M. Vairamani, Chemical characteristics of rainwater at an urban site of south-central India, Atmos. Environ. (2003), https://doi.org/10.1016/S1352-2310(03)00266-8.
[172] D.S. Covert, R.J. Charlson, N.C. Ahlquist, A study of the relationship of chemical composition and humidity to light scattering by aerosols, J. Appl. Meteorol. 2 (1972), https://doi.org/10.1175/1520-0450(1972)011%3C0968:ASOTRO%3E2.0.CO.
[173] S. Tsyro, D. Simpson, L. Tarrasón, Z. Klimont, K. Kupiainen, C.A. Pio, K.E. Yttri, Modeling of elemental carbon over Europe, J. Geophys. Res. Atmos. (2007), https://doi.org/10.1029/2006JD008164.
[174] B.S. Kamber, A. Greig, K.D. Collerson, A new estimate for the composition of weathered young upper continental crust from alluvial sediments, Queensland, Australia, Geochem. Cosmochim. Acta (2005), https://doi.org/10.1016/j.gca.2004.08.020.
[175] T. Moreno, X. Querol, A. Alastuey, J. de la Rosa, A.M. Sánchez de la Campa, M.C. Minguillón, M. Pandolfi, Y. González-Castanedo, E. Monfort, W. Gibbons, Variations in vanadium, nickel and lanthanoid element concentrations in urban air, Sci. Total Environ. (2010), https://doi.org/10.1016/j.scitotenv.2010.06.016.